



On the use of a roving body with rotary inertia to locate cracks in beams



F. Cannizzaro ^a, J. De Los Rios ^b, S. Caddemi ^{a,*}, I. Calì ^a, S. Ilanko ^b

^a Dipartimento Ingegneria Civile e Architettura, Università di Catania, Via Santa Sofia 64, Catania, Italy

^b School of Engineering, University of Waikato, Hamilton, New Zealand

ARTICLE INFO

Article history:

Received 19 May 2017

Received in revised form 9 March 2018

Accepted 15 March 2018

Keywords:

Closed form solution

Rotary inertia

Crack localization

Concentrated damage

Generalised functions

Inverse problems

ABSTRACT

Identifying cracks and damages in structures using measured vibrational characteristics has received considerable attention in the past few decades. The possibility of using frequency changes due to the application of a mass appended to the structure has also been considered. In this paper an analytical proof to show that the natural frequencies of a cracked beam with a roving body possessing mass and rotary inertia will generally change abruptly as the body passes over a crack, provided that the crack permits differential flexural rotations, is presented. A novel explicit closed form solution of the governing equation of an Euler-Bernoulli beam with a roving body possessing mass and rotary inertia, in the presence of multiple cracks is also proposed. The presented exact solution is used to conduct a parametric analysis of cracked beams. Numerical results for natural frequencies are provided and a procedure to exploit the occurrence of frequency shifts to detect and locate each crack, without having to perform any additional calculation, is described.

© 2018 Elsevier Ltd. All rights reserved.

1. Introduction

Structural integrity of engineering constructions and structures is affected by the normal process of deterioration which can compromise their safety and serviceability. In the past few decades many efforts have been taken by engineers to detect and localize damage in its early stage using vibrational measurements as is implicit in the comprehensive literature review on structural health monitoring and damage identification presented by Doebling et al. [1].

Most of the vibration measurements came from acceleration data that have to be processed in order to extract modal parameters, such as the natural frequencies, to characterise the dynamics of the structure. In the words of Doebling et al. [2]: “The vibration based identification methods rely on the fact that damage generates singularities in the modal parameters”.

As mentioned in Ref. [3] only a significant damage would cause a measurable change when the damage detection is carried out by analysing the changes in the natural frequencies and the damage effect could be veiled by environmental changes and experimental uncertainties. To overcome the problem of sensitivity of the changes in natural frequencies, Pandey et al. [4] proposed to use the mode shapes to capture the discontinuity produced by the damage. Mode shapes have also been used to reconstruct position and severity of multiple cracks by proposing a sequential identification

* Corresponding author.

E-mail address: scaddemi@dica.unict.it (S. Caddemi).

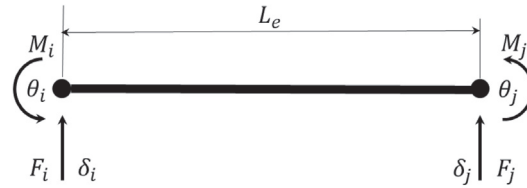


Fig. 1. Sign convention for beam elements.

procedure [5]. However, compared with the natural frequency measurements, the identification of mode shapes requires additional experimental and mathematical resources, and the effect of small damage on the modes is normally of the order of experimental noise and environmental effects, making the identification problem a complicated task [3]. It is worth noting that several identification procedures assume the number of concentrated cracks as a known variable, but in real applications this is not the case. Thus there is a need to develop a reliable identification procedure that is able to detect the exact number and location of the cracked cross sections which is the motivation behind the work presented in this paper.

In order to easily distinguish the changes induced by damage, Zhong and Oyadiji [6] and Solís et al. [3] use wavelet coefficients as an indicator of damage when they are applied to the differences in mode shapes between the undamaged and the damaged beams. It may be noted that Zhong and Oyadiji [6] and Bahador and Oyadiji [7] performed the modal analysis for different positions of a non-structural mass attached to the structure in order to make the damage detection method more robust and sensitive. The roving mass method proposed by Zhong and Oyadiji in Ref. [8] involves locating the mass at different positions at each round of test, but during the vibration measurement the mass is not allowed to move axially, so its velocity effects need not be considered.

In this paper, besides the translational inertia (mass) of the roving body, the effect of its rotational inertia is also taken into account. It should be noted that the rotary inertia due to the self mass of the beam is not considered in this work. That is the beam is an Euler-Bernoulli beam and not a Timoshenko beam. The idea of using the rotary inertia of the roving body is to exploit the fact that, since the damage produces a rotational discontinuity at the crack location, it is expected that the rotary inertia would introduce a jump in the frequency as the roving body crosses the crack position. The theoretical proof of the latter statement and the influence of each of the parameters in the determinantal equation will be discerned following the derivations explained in Ref. [9] using the Dynamic Stiffness Matrix. A procedure, based on the detection of the frequency jumps, that generally enables identification of the number of cracks present in a beam and their location is proposed. The most significant feature of this procedure is that it does not require any knowledge of the dynamic properties of the corresponding healthy beam. Furthermore, a closed form integration of the governing free vibration equations of a multi-cracked beam, in the presence of a roving body with both translational and rotary inertia, is derived to numerically analyse the performance of the proposed identification method aiming at providing a first investigation versus its practical applicability. The results have also been verified by comparing with results obtained using the Finite Element Method.

2. Frequency shift derivation using dynamic stiffness matrix (DSM)

According to the rotational stiffness model, a cracked beam is split at the crack position into two segments which are connected by a hinge allowing a discontinuity in the slope with a partial rotational restraint modelled by a rotational spring of stiffness K which is related to the severity of the damage [10]. The connecting spring is also referred to as a torsional spring but it should be noted that it restrains the relative flexural rotation only and not the angle of twist. When considering only transverse and angular displacements using the dynamic stiffness approach there are two degrees of freedom for vibration in one plane at each end of any beam element of length L_e with the following assumed sign convention, Fig. 1.

The exact dynamic stiffness equations for each beam element with Young's modulus E , second moment of area I and mass per unit length m , vibrating at frequency ω is given in Ref. [11] as follows:

$$\begin{Bmatrix} F_i \\ M_i \\ F_j \\ M_j \end{Bmatrix} = \begin{bmatrix} a_e & b_e & -d_e & e_e \\ b_e & c_e & -e_e & f_e \\ -d_e & -e_e & \alpha_e & -\beta_e \\ e_e & f_e & -\beta_e & \gamma_e \end{bmatrix} \begin{Bmatrix} \delta_i \\ \theta_i \\ \delta_j \\ \theta_j \end{Bmatrix} \quad (1)$$

where, for a uniform member:

$$\begin{aligned}
 a_e &= \alpha_e = \frac{EI\bar{\alpha}^3(s_e C_e + c_e S_e)}{\sigma_e}; b_e = \beta_e = \frac{EI\bar{\alpha}^2 s_e S_e}{\sigma_e}; c_e = \gamma_e = \frac{EI\bar{\alpha}(s_e C_e - c_e S_e)}{\sigma_e}; \\
 d_e &= \frac{EI\bar{\alpha}^3(S_e + s_e)}{\sigma_e}; e_e = \varepsilon_e = \frac{EI\bar{\alpha}^2(C_e - c_e)}{\sigma_e}; f_e = \frac{EI\bar{\alpha}(S_e - s_e)}{\sigma_e}; \\
 \sigma_e &= 1 - c_e C_e; \bar{\alpha} = (m\omega^2/EI)^{0.25}; \\
 s_e &= \sin(L_e\bar{\alpha}); c_e = \cos(L_e\bar{\alpha}); C_e = \cosh(L_e\bar{\alpha}); S_e = \sinh(L_e\bar{\alpha})
 \end{aligned}
 \tag{2}$$

On the other hand, the dynamic stiffness equation for the spring connecting two elements, is given in terms of non-dimensional stiffness $k = \frac{K_L}{EI}$ as follows:

$$\begin{Bmatrix} M_L \\ M_R \end{Bmatrix} = \begin{bmatrix} k & -k \\ -k & k \end{bmatrix} \begin{Bmatrix} \theta_L \\ \theta_R \end{Bmatrix}
 \tag{3}$$

where subscripts L and R indicate cross sections at the left and the right of the spring, respectively. In the rotational spring model, the global dynamic stiffness matrix for a cracked structure is assembled in the usual way as done in the FEM, connecting the individual elements in the structure accordingly at the global degrees of freedom where they are joined.

For the case of a beam of length $L = L_a + L_b$, with both ends fixed and with one crack along its length, Fig. 2, the resulting global stiffness matrix possesses three degrees of freedom at the crack location, the translation of the hinge and the two rotations connected by the spring, and takes the following form:

$$\begin{Bmatrix} M_L \\ F \\ M_R \end{Bmatrix} = \begin{bmatrix} \gamma_a + k & -\beta_a & -k \\ -\beta_a & \alpha_a + a_b & b_b \\ -k & b_b & c_b + k \end{bmatrix} \begin{Bmatrix} \theta_L \\ \delta \\ \theta_R \end{Bmatrix}
 \tag{4}$$

where the subscripts refer to each beam element. It is shown in Ref. [9] that the determinantal equation for any cracked structure can be expressed as:

$$D_0(\omega)k + D_h(\omega) = 0
 \tag{5}$$

Where $D_0(\omega)$ is the determinant of the uncracked structure and $D_h(\omega)$ is the determinant of the structure with a hinge at the crack location. For the case of a clamped-clamped beam with a single crack under consideration, $D_0(\omega)$ and $D_h(\omega)$, provided that the terms with the same denominator are simplified, take the following form:

$$\begin{aligned}
 D_0(\omega) &= 2\bar{\alpha}^4[1 - cC] \\
 D_h(\omega) &= \bar{\alpha}^5[sC_a C_b - SC_a c_b + s_a C_a + s_b C_b - c_a S_a - c_b S_b]
 \end{aligned}
 \tag{6}$$

where $s = \sin(L\bar{\alpha})$ $c = \cos(L\bar{\alpha})$ $C = \cosh(L\bar{\alpha})$ $S = \sinh(L\bar{\alpha})$. If a roving body in the form of a concentrated mass M_o , (with translational inertia only), is located at the crack position, its effect can be represented by a dynamic force associated with the translation of the cracked cross section that effectively alters the corresponding diagonal element of the dynamics stiffness matrix (DSM) in Eq. (4) with the additional term $\bar{m}_o = \frac{\omega^2}{EI}M_o$. Hence, the global stiffness matrix of the clamped-clamped beam with a single crack in the presence of a concentrated mass becomes:

$$\begin{bmatrix} \gamma_a + k & -\beta_a & -k \\ -\beta_a & \alpha_a + a_b - \bar{m}_o & b_b \\ -k & b_b & c_b + k \end{bmatrix}
 \tag{7}$$

The determinant could be expressed now as:

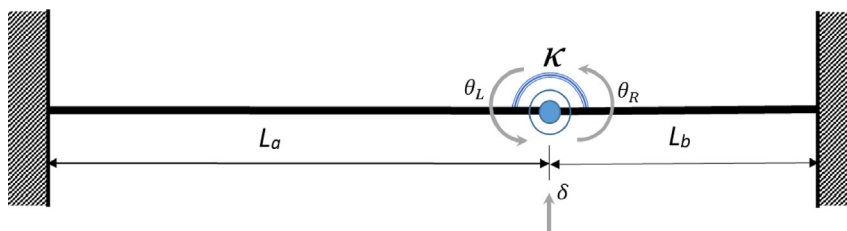


Fig. 2. Rotational spring model of a crack connecting two beam segments.

$$[D_0(\omega) - D_m(\omega)]k + D_h(\omega) + D_{hm}(\omega) = 0, \quad (8)$$

where the additional terms are defined as follows:

$$D_m(\omega) = \frac{M_0 \bar{\alpha}^5}{m} [s_c c_b - s_c a c_b + c_a s_a + c_b s_b - s_a c_a - s_b c_b] \quad (9)$$

$$D_{hm}(\omega) = \frac{M_0 \bar{\alpha}^6}{m} (s_a c_a - c_a s_a)(s_b c_b - c_b s_b)$$

providing that all terms in the characteristic equation (Eq. (8)) with the same denominator are to be simplified.

If there is no crack, the flexibility $k^{-1} = 0$ annuls $D_h(\omega)$ and $D_{hm}(\omega)$, leading to the determinantal equation of an undamaged structure with an added mass with translational inertia as follows:

$$D_0(\omega) - D_m(\omega) = 0 \quad (10)$$

Following the same procedure the effect of a roving body due to its rotary inertia $I_o = e^2 \frac{\omega^2}{EI} M_o$ can be found by adding this term to the corresponding diagonal element of the DSM in Eq. (7) (e being the effective transverse eccentricity of a concentrated mass that will produce the same rotary inertia as that of the body). Precisely, when the added rotary inertia is located at the left side of the spring, the global stiffness matrix of the clamped-clamped beam with a single crack can be given the following form:

$$\begin{bmatrix} \gamma_a + k - I_o & -\beta_a & -k \\ -\beta_a & \alpha_a + a_b - \bar{m}_o & b_b \\ -k & b_b & c_b + k \end{bmatrix} \quad (11)$$

The determinantal equation of the global stiffness matrix in Eq. (11) can be given in the following form:

$$[D_0(\omega) - D_m(\omega) + D_{mr}(\omega) - D_r(\omega)]k + D_h(\omega) + D_{hm}(\omega) + D_{hmr}(\omega) + D_{hr}(\omega) = 0 \quad (12)$$

where the additional terms with respect to the expression in Eq. (8) are derived from the expansion of the quantity $-I_o(\alpha_a + a_b - \bar{m}_o)(c_b + k) - I_o b_b^2$ and are defined as follows:

$$D_{mr}(\omega) = \bar{m}_o I_o (1 - C_a c_a)(1 - C_b c_b) \quad (13)$$

$$D_r(\omega) = I_o \bar{\alpha}^3 [(s_a c_a + c_a s_a)(1 - C_b c_b) + (s_b c_b + c_b s_b)(1 - C_a c_a)] \quad (14)$$

$$D_{hmr}(\omega) = \bar{m}_o I_o \bar{\alpha} (s_b c_b - c_b s_b)(1 - C_a c_a) \quad (15)$$

$$D_{hr}(\omega) = I_o \bar{\alpha}^4 [(s_b c_b - c_b s_b)(s_a c_a + c_a s_a) + (1 + C_b c_b)(1 - C_a c_a)] \quad (16)$$

On the other hand if the body with the rotary inertia is on the right side of the crack, the DSM takes the form:

$$\begin{bmatrix} \gamma_a + k & -\beta_a & -k \\ -\beta_a & \alpha_a + a_b - \bar{m}_o & b_b \\ -k & b_b & c_b + k - I_o \end{bmatrix} \quad (17)$$

where the change in the position of the rotary inertia I_o leads to the term $-I_o(\alpha_a + a_b - \bar{m}_o)(\gamma_a + k) - I_o \beta_a^2$ that affects the expressions of $D_{hmr}(\omega)$ and $D_{hr}(\omega)$, appearing in Eq. (12), now given as follows:

$$D_{hmr}(\omega) = \bar{m}_o I_o \gamma_a = \bar{m}_o I_o \bar{\alpha} (s_a c_a - c_a s_a)(1 - C_b c_b) \quad (18)$$

$$D_{hr}(\omega) = I_o (a_b \gamma_a + \alpha_a \gamma_a - \beta_a^2) = I_o \bar{\alpha}^4 [(s_b c_b + c_b s_b)(s_a c_a - c_a s_a) + (1 - C_b c_b)(1 + C_a c_a)] \quad (19)$$

The expressions of $D_{hmr}(\omega)$ and $D_{hr}(\omega)$, appearing in Eq. (12), take two different expressions depending on whether the roving body is at the left or the right of the crack, i.e. Eqs. (15) and (16) or Eqs. (18) and (19), respectively.

It can be concluded that unlike the translational inertia of the concentrated mass, the effect of a rotary inertia passing a cracked cross section consists in an abrupt change of the determinantal equation and a consequent shift of the natural frequencies. This then leads to a useful implication that the location of a crack could be detected by the presence of a jump in the free vibration frequency measurements for different position of the concentrated roving body.

However, it has to be noted that Eqs. (15) and (16) are identical to Eqs. (18) and (19) if the crack is located at a line of symmetry so that $\alpha_a = a_b$, $\gamma_a = c_b$ and $\beta_a = b_b$ and the determinant in Eq. (12) will not suffer any change. In the latter case no

frequency shift is encountered as the crack is crossed by a body with rotary inertia, that can be considered an exception to the general property.

Furthermore, it is also worth to notice that different expressions of $D_{hr}(\omega)$ and $D_{hmr}(\omega)$ have an effect on the determinant only when the rotational spring flexibility is non-zero (i.e. there is a crack). In other words, no frequency shift appears in absence of a crack.

Finally, it can be stated that the inertial terms $D_{hr}(\omega)$ and $D_{hmr}(\omega)$, dependent on the rotary inertia I_o affected by the squared frequency, will have a noticeable change especially at high frequencies, even with low values of rotary inertia.

A damage location procedure can hence be more efficaciously conducted by measuring the frequency shift at high frequencies.

3. Frequency shift evidence by observation of the cracked beam mode shapes

A further evidence of the effect of a body possessing rotary inertia on the natural frequencies of a beam as it moves across a crack can be clearly seen by the analysis of the relevant vibration modes. Abrupt changes of the mode shapes of the cracked beam will be generally exhibited when the two body positions located immediately to the left and right of the crack are considered. The two different vibration mode shapes, related to a body located immediately to the left and right of the crack, are characterised by different end conditions for the two beam segments which explains the frequency shift highlighted analytically in the previous section.

For the above purpose let us consider a clamped-clamped beam with a single crack, modelled by a hinge with a rotational spring (specific data are reported in Table 1), in the presence of a roving body located just before and after the cracked section of a clamped-clamped beam. Without loss of generality, to better highlight the above mentioned changes, in Fig. 3 the first six vibration modes and the relevant frequencies are reported for the special case of the roving body characterised by a large translational inertia (compared to the self mass of the beam) and an associated rotary inertia which is also large.

Generally speaking, Fig. 3 shows that the vibration modes can be of two different types: *i*) modes implying vibrations of both segments of the beam divided by the crack (i.e. global modes involving the entire beam); *ii*) local vibrations modes involving a single segment of the beam while the second segment has negligible contribution to the vibration mode.

In the first type *i*), where both beam segments participate in vibration, the appended roving body also vibrates. Since the mass of the appended body is much larger than the mass of the beam, the beam mass can be neglected resulting effectively in a 2 dofs system, where the beam segments provide elastic stiffness only. There are only two such modes and due to the relatively large mass and rotary inertia these have very low natural frequencies. On the other hand, for all other modes (type *ii*), the appended body acts like a constraint and effectively separates the two beam segments. The constraining effect of large mass and rotary inertia has been proven in Ref. [12]. This means that one side of the beam does not participate significantly in the vibration whereas the other undergoes natural vibration (see modes from three up to six in Fig. 3). The latter behaviour can be explained by noting that when the body is located at the left of the crack (graphs in the left column of Fig. 3), due to its large inertia, the left segment of the beam tends to vibrate as a clamped-clamped beam of length 0.7 while the beam segment at the right of the crack as a rotational spring restrained-clamped beam of length 0.3.

On the contrary, when the body is located at the right of the crack (graphs in the right column of Fig. 3), the left segment of the beam tends to vibrate as a clamped –rotational spring restrained beam of length 0.7 while the beam segment at the right of the crack as a clamped-clamped beam of length 0.3.

Infact, the theoretical frequencies of undamaged clamped-clamped (c-c) and rotational spring restrained-clamped (rot.-spring-c) beams with lengths 0.3 and 0.7 are reported in red, for comparison, next to those graphs where the correspondent modes of the cracked beam are recovered.

In effect, the large inertia of the body, in terms of natural vibration modes, except the first two modes, separates the two sides of the beam. Thus the natural frequencies for the modes of the two segments of the beam will differ, as the modes are different, indicating a sudden shift in the frequency.

However, the above demonstration regarding the limit behaviour, shown in Fig. 3 from the third frequency onward just to provide further evidence of the frequency jump, does not mean that even the first two frequencies are not affected by frequency jumps. Indeed the frequency shift has been found even for the first two modes.

Table 1
Characteristics of the single cracked beam in Fig. 3.

Young's modulus E	210000 MPa
Density ρ	7500 kg/m ³
Length L	10 m
Height h	0.1 m
Width	1 m
Crack abscissa x_l	7 m
Normalized crack depth d/h	0.6837
Mass of the roving body M_o	375000 Ns ² /m
Eccentricity of the roving body e	1 m

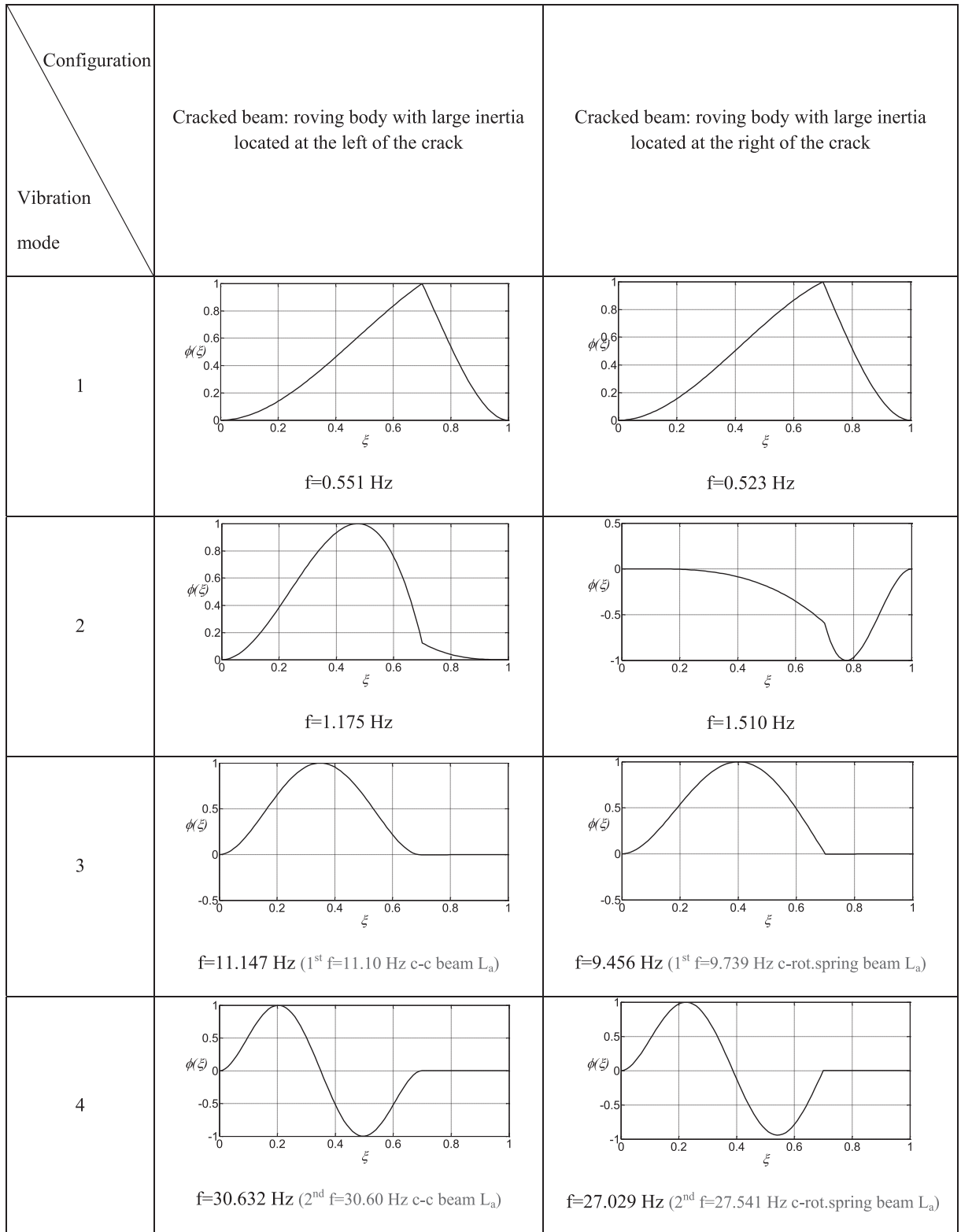


Fig. 3. Vibration modes $\phi(\xi)$ versus normalized abscissa ξ and fundamental frequencies of the clamped-clamped beam described in Table 1 with a single crack in presence of a roving body with large inertia located at the left (second column) and the right (third column) of the crack.

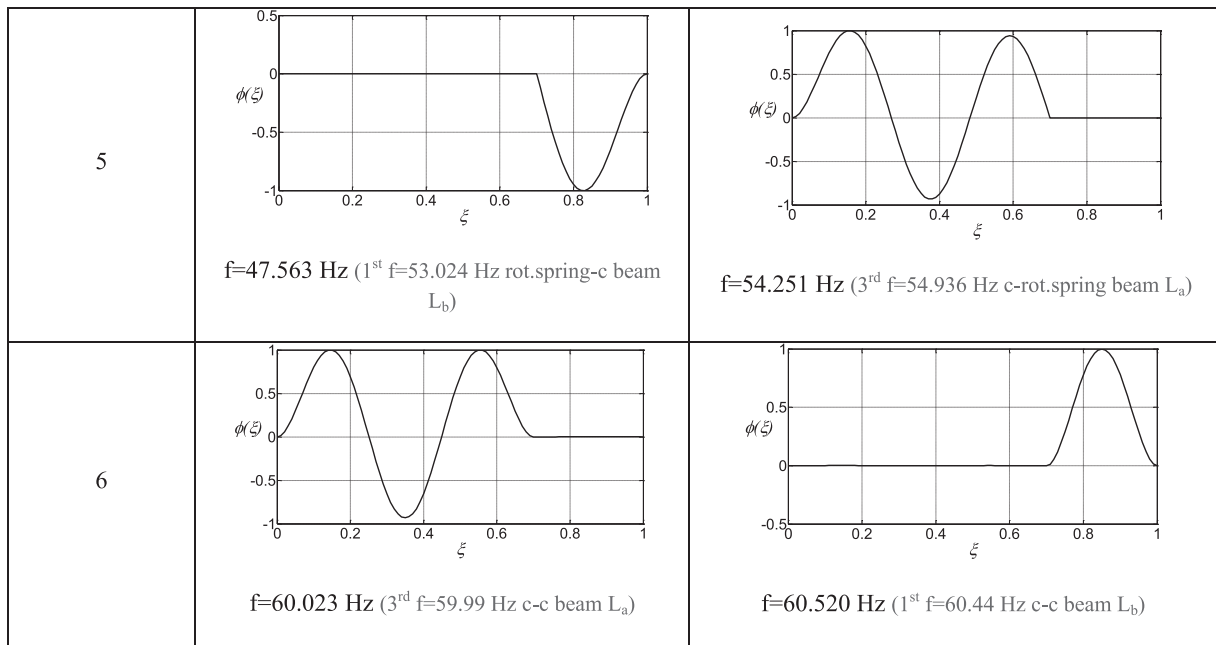


Fig. 3. (continued).

This sudden change in the frequency is due entirely to the presence of the attached body with rotary inertia. This example regarding a roving body with large inertia is presented only as an illustration to show that as a body possessing inertia moves across a point of discontinuity in the slope of the beam deflection (i.e. a crack), there is an associated change to the mode shapes and thus frequencies. Even if the translatory and rotary inertia are not of large magnitude, there will be a sudden change in the frequencies, as well as the associated mode shapes, as the body moves across a crack. The only exceptions occur where the crack is at the centre of a symmetrical beam, in which case while the actual modes of each side of the crack will swap sides, the natural frequencies will not change.

4. The governing equations of multi-cracked beams with a roving mass possessing rotary inertia effect: closed form solution

In Section 2 the DSM method has been employed to provide a general proof that the presence of rotary inertia modifies the determinantal equation when the roving body passes over a crack. However, when a multi-cracked beam is considered, the construction of the relevant DSM requires a recurrent and cumbersome procedure. For this reason a model and a relevant solution strategy of the governing equations of a beam with a roving body, based on generalised functions, is employed here for the numerical applications. The use of generalised functions, already adopted by some of the authors for cracked beams with no additional masses [13–17], is extended here to account for the presence of a roving body with translational and rotary inertia. The solution, proposed in explicit closed form, is unique and is provided in terms of four (boundary conditions dependent) integration constants only, that, unlike in the classic DSM approach, does not require any additional node, or continuity condition, at the cracked sections and at the roving body location.

The frequency shifts of a cracked beam induced by a concentrated roving body at the body, discussed in the previous sections for crack location purposes, can be easily studied by means of the proposed closed form solution presented in this section.

Let us consider an Euler-Bernoulli beam, with a spatial abscissa x spanning from 0 to the length L and distributed mass m , in presence of multiple cracks at x_i , $i = 1, \dots, n$, and an additional concentrated mass M_o with an eccentricity e at x_o . The presence of a body of mass M_o along a beam axis, besides inducing a translational inertial force, activates also a rotational contribution accounting for the rotary inertia effect, that can be represented by placing two concentrated masses of magnitude $M_o/2$ at an eccentricity e , thus providing an inertia of $M_o e^2$, as shown in Fig. 4.

The governing equation of vibratory motion of the beam in terms of deflection function $v(x, t)$, with t time variable, is written as follows:

$$\begin{aligned}
 v^{IV}(x, t) - \frac{M_0 e^2}{EI} [\delta^I(x - x_0) \dot{v}^I(x_0, t)] + \frac{m}{EI} \left[1 + \frac{M_0}{m} \delta(x - x_0) \right] \ddot{v}(x, t) = \\
 = \sum_{i=1}^n \Delta v(x_i, t) \delta^{II}(x - x_i)
 \end{aligned}
 \tag{20}$$

where $\delta(\bullet)$ is the well known Dirac's delta distribution and the superimposed dot and the apex indicate temporal and spatial differentiation, respectively.

Eq. (20) has been specially devised to account for the influence of rotary inertia and translational inertia of the body by means of the terms $-\frac{M_0 e^2}{EI} [\delta^I(x - x_0) \dot{v}^I(x_0, t)]$ and $\frac{M_0}{EI} \delta(x - x_0) \ddot{v}(x, t)$, respectively. Furthermore, the summation term on the right side of Eq. (20) is due to the influence of the unknown rotational discontinuities $\Delta v^I(x_i, t)$ at the cracked cross sections.

By introducing the normalized abscissa $\xi = x/L$ and the normalized deflection normalized deflection function $u(\xi, t) = v(x, t)/L$, the corresponding normalized governing equation is obtained:

$$\begin{aligned}
 u^{IV}(\xi, t) - \frac{mL^4}{EI} \frac{M_0}{mL} \frac{e^2}{L^2} \delta^I(\xi - \xi_0) \dot{u}^I(\xi_0, t) + \frac{mL^4}{EI} \left[1 + \frac{M_0}{mL} \delta(\xi - \xi_0) \right] \ddot{u}(\xi, t) = \\
 = \sum_{i=1}^n \Delta u^I(\xi_i, t) \delta^{II}(\xi - \xi_i)
 \end{aligned}
 \tag{21}$$

where the unknown rotational discontinuities $\Delta u^I(\xi_i, t)$ can be related to the second derivative of the normalized deflection function, by accounting for the spring rotational stiffness K_i equivalent to the cracks, as follows:

$$\Delta u^I(\xi_i, t) = \frac{EI}{K_i} \frac{1}{L} u^{III}(\xi_i, t) = \lambda_i u^{II}(\xi_i, t)
 \tag{22}$$

with $\lambda_i = K_i^{-1}$ being the normalized crack compliance. By imposing in Eq. (21) the separation of variables, the normalized deflection function can be assumed as the product of the vibration mode $\phi(\xi)$ depending on the spatial coordinate ξ , representing the vibration mode, and a time dependent function $y(t)$ as follows $u(\xi, t) = \phi(\xi)y(t)$. The following fourth-order equation in terms of vibration mode $\phi(\xi)$ can be inferred:

$$\begin{aligned}
 \phi^{IV}(\xi) - \alpha^4 \phi(\xi) = \alpha^4 m_0 \phi(\xi_0) \delta(\xi - \xi_0) + \\
 - \alpha^4 m_0 e^2 \delta^I(\xi - \xi_0) \phi^I(\xi_0) + \sum_{i=1}^n \lambda_i \phi^{II}(\xi_i) \delta^{II}(\xi - \xi_i)
 \end{aligned}
 \tag{23}$$

where $\alpha^4 = \omega^2 \frac{mL^4}{EI} = (\bar{\omega}L)^4$ is the frequency parameter. Furthermore, in Eq. (23), $m_0 = \frac{M_0}{mL}$ represents the concentrated mass normalized with respect to the beam mass density and the beam length, and $\epsilon = \frac{\xi}{L}$ is the eccentricity of the mass normalized with respect to the beam length. Eq. (23) can be straightforwardly and efficaciously integrated by employing the Laplace transform procedure to deal with the terms containing generalised functions. The solution, whose derivation is reported in the Appendix, is provided in an explicit form as follows:

$$\phi(\xi) = C_1 f_1(\xi, \alpha) + C_2 f_2(\xi, \alpha) + C_3 f_3(\xi, \alpha) + C_4 f_4(\xi, \alpha)
 \tag{24}$$

where

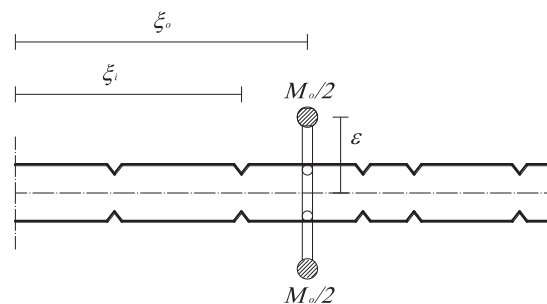


Fig. 4. Multi-cracked beam with roving body with mass and rotary inertia represented by concentrated masses at eccentricity ϵ .

$$f_j(\xi, \alpha) = h_j(\xi, \alpha) + \bar{h}_0(\xi, \alpha)\alpha^4 m_0 f_j(\xi_0, \alpha) + \bar{h}_R(\xi, \alpha)\alpha^4 m_0 \varepsilon^2 f_j^I(\xi_0, \alpha) + \sum_{k=1}^n \bar{h}_k(\xi, \alpha) \lambda_k f_j^{II}(\xi_k, \alpha), j = 1, \dots, 4 \tag{25}$$

and

$$\begin{aligned} h_1(\xi, \alpha) &= \sin \alpha \xi; & h_2(\xi, \alpha) &= \cos \alpha \xi; & h_3(\xi, \alpha) &= \sinh \alpha \xi; & h_4(\xi, \alpha) &= \cosh \alpha \xi; \\ \bar{h}_0(\xi, \alpha) &= \frac{1}{2\alpha^3} [-\sin \alpha(\xi - \xi_0) + \sinh \alpha(\xi - \xi_0)]U(\xi - \xi_0) \\ \bar{h}_R(\xi, \alpha) &= \frac{1}{2\alpha^2} [\cos \alpha(\xi - \xi_0) - \cosh \alpha(\xi - \xi_0)]U(\xi - \xi_0) \\ \bar{h}_i(\xi, \alpha) &= \frac{1}{2\alpha} [\sin \alpha(\xi - \xi_i) + \sinh \alpha(\xi - \xi_i)]U(\xi - \xi_i) \end{aligned} \tag{26}$$

In particular, the functions $h_j(\xi, \alpha)$, $j = 1, \dots, 4$, represent the solution of the homogeneous beam, while $\bar{h}_0(\xi, \alpha)$, $\bar{h}_R(\xi, \alpha)$, $\bar{h}_i(\xi, \alpha)$, $i = 1, \dots, n$, represent additional functions able to account for the presence respectively of the translational mass, the rotary inertia, and the cracks.

The integration constants appearing in the solution in Eq. (10) can be obtained by imposing the relevant boundary conditions. In particular, for the case of a clamped-clamped beam which is fully analyzed in the following applications, the boundary conditions are as follows:

$$\phi(0) = 0; \quad \phi^I(0) = 0; \quad \phi(1) = 0; \quad \phi^I(1) = 0 \tag{27}$$

Enforcing the boundary conditions in Eq. (24) the following determinantal equation, subject to the conditions $C_1 = -C_3$ and $C_2 = -C_4$, can be derived:

$$[f_3(1, \alpha) - f_1(1, \alpha)] [f_4^I(1) - f_2^I(1, \alpha)] - [f_4(1, \alpha) - f_2(1, \alpha)] [f_3^I(1, \alpha) - f_1^I(1, \alpha)] = 0 \tag{28}$$

Eq. (28), in view of Eqs. (25) and (26), is the generalised function counterpart of the expression in Eq. (12) formulated by means of the DSM approach.

Eq. (28) can be solved numerically in terms of the frequency parameter α . The roots of the equation provide the fundamental frequencies of the beam, and allow computation of the integration constants and derivation of the corresponding mode shapes.

Based on Eq. (28), it can again be proven that the determinantal equation of a cracked beam undergoes an abrupt change when a body possessing rotary inertia crosses a crack, indicating the occurrence of a frequency jump.

In fact, for the case of a clamped-clamped beam with a single crack ($n = 1$) at ξ_1 , the $f_j(1, \alpha)$ functions and their first derivatives appearing in Eq. (28) can be written as:

$$\begin{aligned} f_j(1, \alpha) &= h_j(1, \alpha) + \bar{h}_0(1, \alpha)\alpha^4 m_0 f_j(\xi_0, \alpha) + \bar{h}_R(1, \alpha)\alpha^4 m_0 \varepsilon^2 f_j^I(\xi_0, \alpha) + \bar{h}_c(1, \alpha)\lambda_1 f_j^{II}(\xi_1, \alpha), \quad j = 1, \dots, 4 \\ f_j^I(1, \alpha) &= h_j^I(1, \alpha) + \bar{h}_0^I(1, \alpha)\alpha^4 m_0 f_j(\xi_0, \alpha) + \bar{h}_R^I(1, \alpha)\alpha^4 m_0 \varepsilon^2 f_j^I(\xi_0, \alpha) + \bar{h}_c^I(1, \alpha)\lambda_1 f_j^I(\xi_1, \alpha), \quad j = 1, \dots, 4 \end{aligned} \tag{29}$$

where $f_j(\xi_0, \alpha)$, $f_j^I(\xi_0, \alpha)$, $f_j^I(\xi_1, \alpha)$ depend on whether the roving body is located before or beyond the crack. In particular the latter terms take the following form:

$$\begin{aligned} f_j(\xi_0, \alpha) &= h_j(\xi_0, \alpha), \\ f_j^I(\xi_0, \alpha) &= h_j^I(\xi_0, \alpha), \quad j = 1, \dots, 4 \\ f_j^I(\xi_1, \alpha) &= h_j^I(\xi_1, \alpha) + \bar{h}_R^I(\xi_1, \alpha)\alpha^4 m_0 \varepsilon^2 f_j^I(\xi_0, \alpha) \end{aligned} \tag{30}$$

when the roving body is located on the left of the crack (i.e. $\xi_0 = \xi_1^-$), while they take the following form

$$\begin{aligned}
 f_j(\xi_o, \alpha) &= h_j(\xi_o, \alpha), \\
 f_j^I(\xi_o, \alpha) &= h_j^I(\xi_o, \alpha) + \bar{h}_1^I(\xi_o, \alpha) \lambda_1 f_j^{II}(\xi_1, \alpha), \quad j = 1, \dots, 4 \\
 f_j^{II}(\xi_1, \alpha) &= h_j^{II}(\xi_1, \alpha)
 \end{aligned}
 \tag{31}$$

when the mass is on the right of the crack (i.e. $\xi_o = \xi_1^+$).

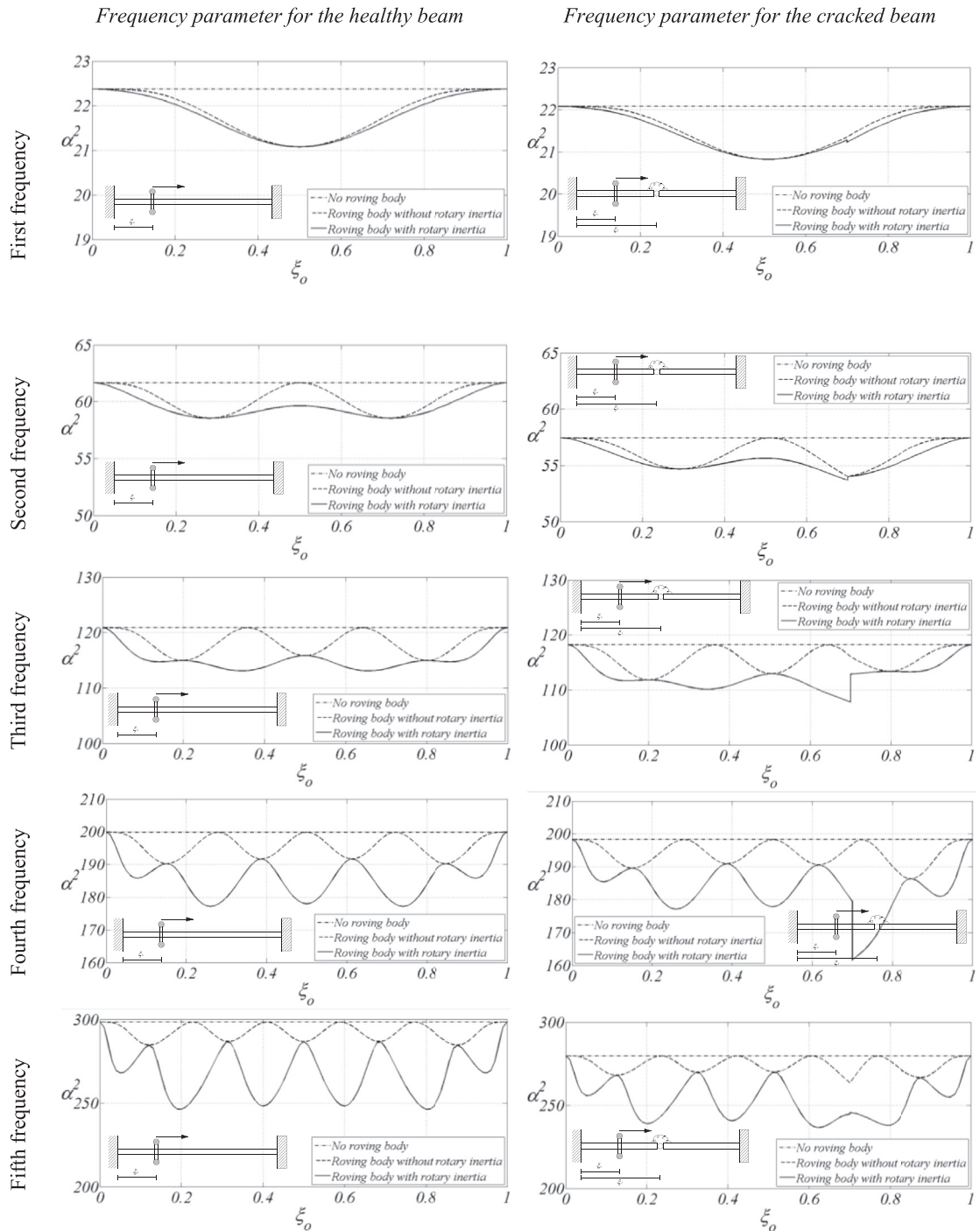


Fig. 5. Frequency parameter α^2 vs position of the roving body for the first five frequencies: healthy (left column) and cracked (right column).

Comparing Eqs. (30) and (31), accounting for the definitions in Eqs. (25) and (26), reveals that the functions $f_j^I(\xi_0, \alpha)$, $f_j^{II}(\xi_1, \alpha)$ change in view of additional terms, depending on whether the roving body is on the left or the right side of the crack. Hence, this reaffirms the finding in the previous section, that the discontinuous form of the determinantal equation (28), when the mass crosses a crack position, is strictly due to the presence of the rotary inertia and leads to the occurrence of frequency shifts.

Without any loss of generality, while only the boundary conditions relative to clamped-clamped beams are employed in this paper; the achieved conclusions do not depend on the considered boundary conditions.

5. Results and discussions

As proven in Section 2 the presence of a roving body with rotary inertia is able to provide an abrupt jump of the natural frequencies as the body crosses each crack. In principle, any sudden change in the measurement of the first fundamental frequency is sufficient to detect the crack positions. However it will be shown in this section that, accounting for higher frequencies, enhances the effect of cracks. In particular, in this section a numerical investigation of a beam with multiple cracks in the presence of a roving body is conducted based on the explicit solution formulated in Eq. (28). The presented numerical investigation leads to the proposal of a crack detection procedure relying on the existence of jumps affecting the natural frequencies, to be measured by free vibration tests, as the body changes its position along the beam span. A brief summary of the results of the numerical investigation, for a demonstrative purpose only, is also provided in Ref. [18] where only a synthetic description lacking of any proof, validation and exhaustive explanation is reported.

In the first sub-section, the case of a clamped-clamped single cracked beam is analyzed to provide numerical evidence of the frequency shift caused by the rotary inertia as the body crosses the crack. In the second sub-section the same case study is treated by means of two different FE strategies to provide evidence that the property here explored does not depend on the adopted model. In addition, in the third sub-section the sensitivity of the frequency jumps to some significant parameters is investigated and a cumulative frequency measure is proposed to magnify the frequency jump which might not be evident when only a single frequency is accounted for. Then, the case of a beam with two cracks is considered in order to show that the considered procedure is not limited to single cracked beams and that the main feature of the proposed detection procedure, that a sudden change in the frequencies occurs as a body possessing rotary inertia passes a crack, is maintained. Finally, an application to a multi-cracked beam is presented to demonstrate the efficacy of the proposed closed form solution and the detection procedure even in a beam with several cracks.

5.1. Single cracked beam

The case of a clamped-clamped beam with a single crack located at $\xi_1 = 0.7$ is presented here. The crack severity is $\lambda_1 = 0.1$, while the normalized concentrated mass and eccentricity are $m_o = 0.05$ and $\varepsilon = 0.1$, respectively. In Fig. 5 the first five fundamental frequencies (in terms of the frequency parameter α^2) are presented as a function of the position of the roving body ξ_0 . Two different conditions of the beam, namely healthy (left column) and cracked (right column) are considered, for three different cases: 1. beam without any concentrated roving body (dash dot line); 2. beam with a concentrated body with rotary inertia effect neglected (dashed line); 3. beam with a body possessing rotary inertia (continuous line).

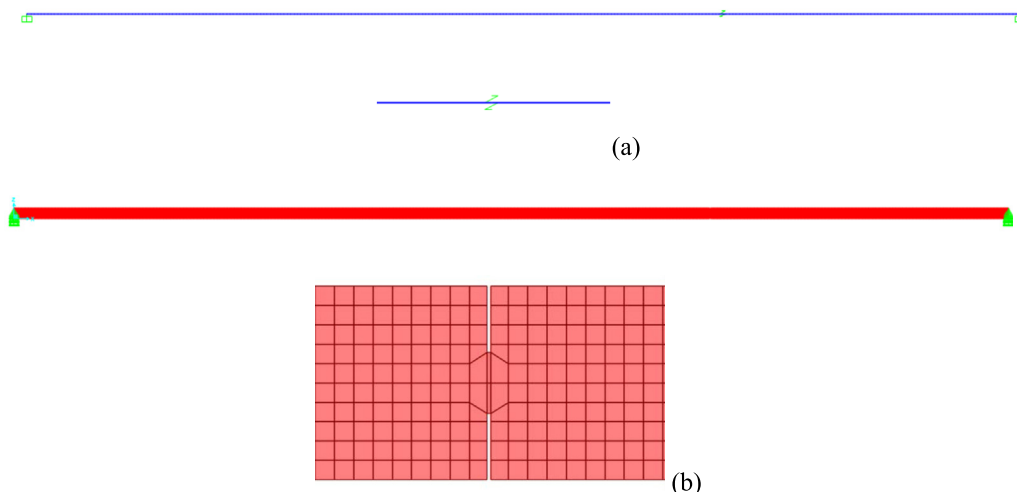


Fig. 6. Adopted FE models with the corresponding crack modelling strategies: (a) FE beam model and (b) FE plane model.

It may be noted that the crack has caused a reduction in the natural frequencies for all modes, irrespective of the location of the roving body and, as expected, for each considered configuration the frequency curve, when the rotary inertia effect of the roving body is neglected, is bounded from above and below by the cases with no additional body and that relative to the roving body with rotary inertia included, respectively.

In particular, the presence of the translational body without rotary inertia causes a first derivative discontinuity in the frequency curve as the mass position coincides with the crack location, as already shown in Ref. [19]. However, this property is hardly recognizable and is considered not suitable for crack location purposes unless wavelet transform is applied to the measured signal to enhance any sort of irregularity [6,20–24].

On the contrary, as shown in Fig. 5, as the main novelty of the present study, for all considered modes, there is a sudden jump in the frequency vs location of the roving body plot as the body possessing rotary inertia passes the crack. It has to be remarked that such jumps have never been encountered in literature in applications regarding beams subjected to a roving body such as in Ref. [25]. In the latter paper, in fact, although the rotary inertia of the self mass of the beam was considered, which is different from the present study, no rotary inertia of any attached rigid body was included in the analysis.

5.2. Frequency jump assessment by means of FE modelling

In order to validate the proposed approach, the same application reported in the previous section is repeated here by means of FE modelling. A set of dimensional parameters equivalent to the dimensionless counterpart reported in Section 5.1 are obtained by using a beam of length $L = 10$ m, with a square cross-section of side length $h = 0.1$ m. The beam is made of a material with Young's modulus $E = 210000$ MPa, and density $\rho = 7500$ kg/m³. The damage is located at the abscissa $x_1 = 7$ m, and is characterised by a symmetric notch whose depth ratio is given by $d/h = 0.6837$. To locate the damage a concentrated mass $M_o = 375$ Ns²/m (corresponding to $m_o = 0.05$ i.e. 5% of the self-mass of the beam) with an eccentricity equal to $e = 1$ m with respect to the axis of the beam is employed.

Two FE modelling strategies have been adopted, as reported in Fig. 6. The numerical results, together with results from the analytical approach, have been presented in Table 2. The FE models have been implemented in the well known software SAP2000 [26] which employs a mass matrix based on concentrated mass and static shape functions; for the latter reason in this case a high mesh resolution is needed to get reliable results. The first model has been implemented by means of beam elements with an equivalent elastic hinge located at the cracked section, whose stiffness is equal to $K = 17500000$ Nm and has been calibrated according to [27]; this first model, addressed in the following as *FE beam model*, is equivalent to the proposed approach in terms of hypotheses related to the crack but is not a closed form solution, and has been implemented to validate numerically the proposed approach. The second model, addressed in the following as *FE plane model*, was implemented by means of bi-dimensional elements, with a mesh size equal to 0.01 m; in this case the crack was modelled by means of a symmetric notch (with a total depth equal to $d = 0.06837$ m), as shown in Fig. 6b. In order to avoid the creation of a more complex structure, the roving body has been modelled by simply assigning two additional translational concentrated masses at the extrados and intrados nodes of the desired cross section (i.e. the eccentricity of each mass with respect to the beam axis is $h/2$, being h the height of the beam). The rotary inertia of the body results from the eccentricity of the two translational masses acting in the horizontal direction. In particular, different values of inertias, M_h and M_v , can be assigned to the horizontal and vertical directions, respectively. In particular, the vertical component of the translational inertia is related to the mass of the roving body according to the relation $M_v = M_o/2$. On the other hand, in order to reproduce the desired rotary inertia in a simple way, the translational masses in the horizontal direction have been assigned as $M_h = 2M_o e^2/h^2$.

By doing so, the masses added to the FEM model do not lead to a more complex structure, while the features such as the modal shapes change with respect to the bare beam and the frequency jumps as the body passes from the left to right of the crack are still retained.

Table 2
Frequency jumps at the cracked sections for all the considered models.

			Proposed model	FE beam model	FE shell model
Frequency	1	$\omega(\xi_1^-)$ [rad/s]	32.51	32.50	32.68
		$\omega(\xi_1^+)$ [rad/s]	32.43	32.44	32.63
		$\Delta\bar{\omega}$ [%]	0.24	0.20	0.18
2	$\omega(\xi_1^-)$ [rad/s]	82.00	82.02	84.28	
	$\omega(\xi_1^+)$ [rad/s]	82.43	82.49	84.63	
	$\Delta\bar{\omega}$ [%]	0.60	0.58	0.42	
3	$\omega(\xi_1^-)$ [rad/s]	164.65	164.70	165.87	
	$\omega(\xi_1^+)$ [rad/s]	172.41	172.43	172.24	
	$\Delta\bar{\omega}$ [%]	4.60	4.59	3.77	
4	$\omega(\xi_1^-)$ [rad/s]	274.11	274.37	270.36	
	$\omega(\xi_1^+)$ [rad/s]	246.82	246.98	248.54	
	$\Delta\bar{\omega}$ [%]	10.48	10.51	8.41	
5	$\omega(\xi_1^-)$ [rad/s]	373.53	373.55	381.03	
	$\omega(\xi_1^+)$ [rad/s]	374.87	374.89	378.05	
	$\Delta\bar{\omega}$ [%]	0.36	0.36	0.79	

Since no experimental test was available in the literature according to the proposed strategy, the latter approach can be regarded as an alternative to an experimental campaign. To this regard, two comments can be made: i) a different model can be considered as presence of uncertainties in many respects (for example, effective stiffness and inertial properties); ii) since the proposed strategy is based on simple detection of a frequency jump due to the roving body and no jump is expected as effect of the noise, it can be straightforwardly stated that any noise, corrupting the frequency measurements, will not affect the crack detection procedure.

In Fig. 7 the first five fundamental frequencies (in terms of the frequency parameter α^2) relative to the cracked condition (see Fig. 5, right column) are presented as a function of the position of the roving body ξ_0 . The mass matrix assembly, being based on a concentrated mass strategy, implies that, when the 1D beam-model is considered no rotary inertia of beam arises in view of the horizontal alignment of all the nodes. On the contrary, when the 2D plane elements are considered for the beam discretisation, the spatial distribution of the nodes with respect to the beam axis allows the effect of the rotary inertia of the

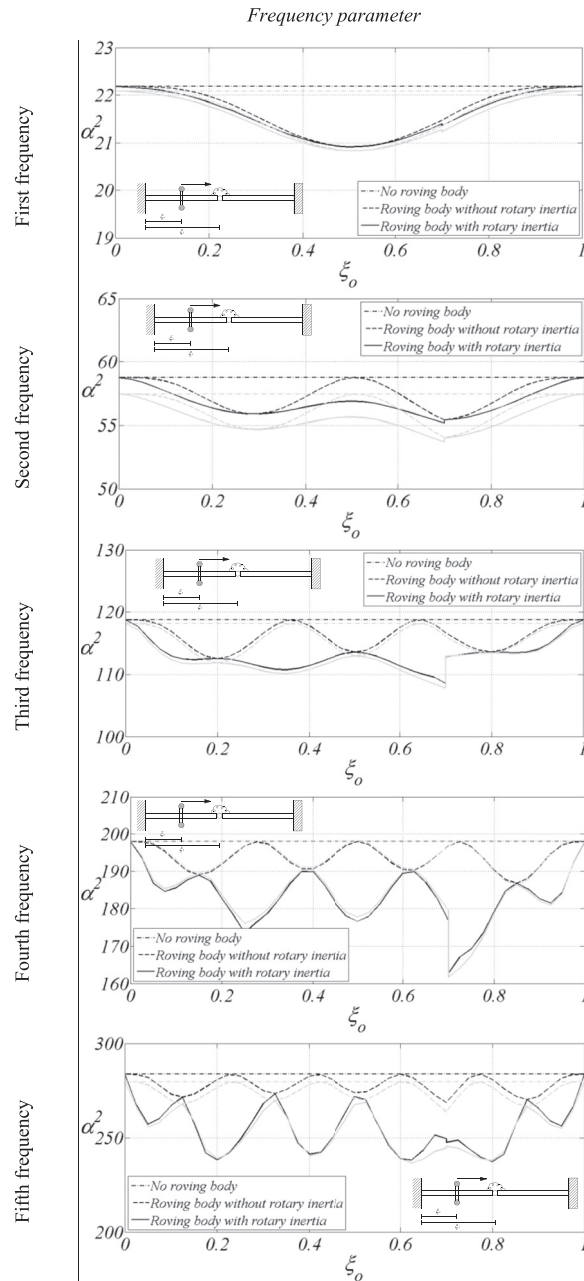


Fig. 7. FEM results in terms of frequency parameter α^2 vs position of the roving body for the first five frequencies for a single cracked beam: FE beam model (black lines) and FE plane model (grey lines).

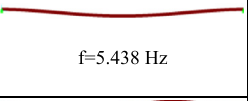
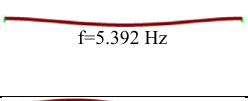
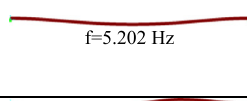
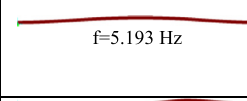
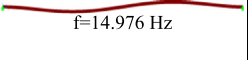
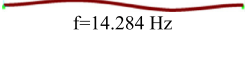
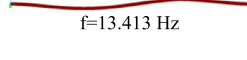
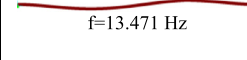
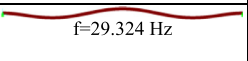
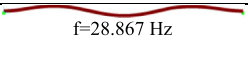
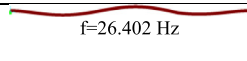
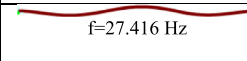
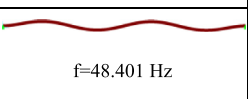
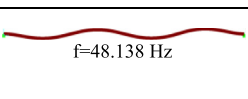
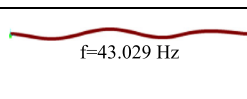
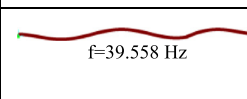
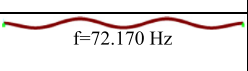
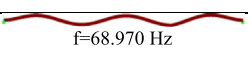
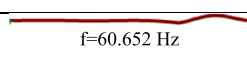
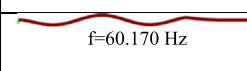
Configuration Mode	Healthy (no additional body)	Cracked (no additional body)	Cracked (additional body endowed with translational and rotary inertia located at the left of the crack)	Cracked (additional body endowed with translational and rotary inertia located at the right of the crack)
1	 $f=5.438$ Hz	 $f=5.392$ Hz	 $f=5.202$ Hz	 $f=5.193$ Hz
2	 $f=14.976$ Hz	 $f=14.284$ Hz	 $f=13.413$ Hz	 $f=13.471$ Hz
3	 $f=29.324$ Hz	 $f=28.867$ Hz	 $f=26.402$ Hz	 $f=27.416$ Hz
4	 $f=48.401$ Hz	 $f=48.138$ Hz	 $f=43.029$ Hz	 $f=39.558$ Hz
5	 $f=72.170$ Hz	 $f=68.970$ Hz	 $f=60.652$ Hz	 $f=60.170$ Hz

Fig. 8. First five mode shapes and fundamental frequencies obtained with the FE plane model with different conditions.

beam and strictly speaking does not respect the Euler-Bernoulli condition. However, this only reinforces the demonstration concerning the frequency shift associated with rotary inertia of the roving body: the shifts are present even for Timoshenko beams. The reason is that the rotary inertia of the roving body effectively changes the boundary conditions of the two beam segments and is independent of the beam theory used.

Numerous analyses have been conducted, with the additional roving mass placed at uniformly spaced points along the beam with a dimensionless step size equal to 0.025 (i.e. 25 cm or at 40 uniformly spaced intervals in the beam), that corresponds to every 25 shell elements, except with the dimensionless interval 0.002 (i.e. 2 cm) in the proximity of the cracked cross section to enhance the effect of the roving body and capture the frequency jump. The same three different cases treated in the previous section are considered: 1. no additional body; 2. additional body without rotary inertia; 3. additional body with rotary inertia; analyzed by means of both FE beam and FE plane models. The results relative to the FE beam models are almost coincident with those obtained with the proposed approach and reported in Fig. 5, left column, thus demonstrating the consistency and reliability of the adopted generalised strategy. There is some discrepancy between the results obtained using the two different FE model and this may be attributed to the differences in the beam self mass distribution and explains the lower frequency shown by the 2D plane elements discretisation. More in general, discrepancies between the two FE models can be found in stiffness and mass properties of the beams and partly due to the differences in the way the crack is modelled. These are in effect similar to experimental noise.

Again, the sudden jump in the frequency as the body possessing rotary inertia passes over the crack is clear for all the adopted models and, even in the case where the largest differences in terms of computed frequencies between the proposed approach and the FE plane model are encountered (i.e. the second frequency), the qualitative property of the frequency jump is clearly recognizable. The results clearly show that irrespective of the method used, there is a sudden frequency shift as a body with rotary inertia passes a crack, which is the main contribution from this work. Again, the mode shapes are strongly influenced by the presence of the roving body endowed with rotary inertia. In Fig. 8, for sake of completeness, the first five modes and the relevant dimensional frequencies are reported for the case of the plane FE model. In particular four scenarios are considered:

- healthy beam without any additional roving body (first column);
- cracked beam without any additional roving body (second column);
- cracked beam with a roving body possessing translational and rotary inertias located at the left of the crack (third column);
- cracked beam with a roving body possessing translational and rotary inertias located at the right of the crack (fourth column).

The results clearly show the frequency jump as the roving body passes over the crack (especially for the third and fourth frequencies) and, more generally, how the presence of the additional inertia tends to enforce different external conditions for the two segments of the beam.

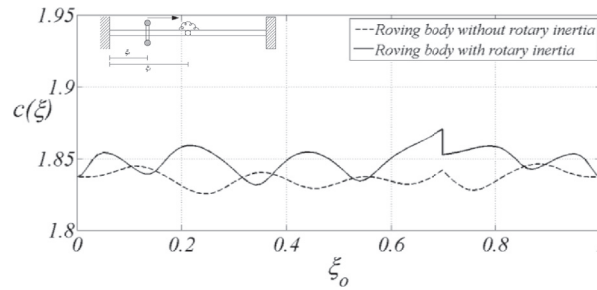


Fig. 9. Single cracked clamped-clamped beam ($\xi_1 = 0.7, \lambda_1 = 1$), variable position of the roving body ($m_o = 0.05, \varepsilon = 0.1$): cumulative frequency parameter for the first five frequencies.

In some cases, for example in the first, second and fifth frequencies, the jump is not very pronounced and may be difficult to be identified; this condition mainly occurs when the crack is located close to a node for a given mode. However, to address this, a method to account for the cumulative effect of several frequencies will be provided in the next section.

In addition, the observed jumps normalized with respect to the average frequency value defined as $\Delta\bar{\omega} = 2 \frac{|\omega(\xi_1^+) - \omega(\xi_1^-)|}{\omega(\xi_1^+) + \omega(\xi_1^-)}$ and reported in Table 2, are larger than the usual frequency measurement precision [28]. Table 2, also shows that the sudden frequency shifts generally increase with mode number. This is due to the fact that the effect of the rotary inertia, namely the rotational moment, is also a product of the square of the natural frequency.

5.3. A cumulative frequency measure and parametric analyses

As mentioned earlier, the jump in the natural frequency can be very small for some of the modes. Therefore, as an alternative, the adoption of a cumulative frequency parameter is suggested as follows:

$$c(\xi_o) = \frac{\sum_{i=1}^{n_f} \alpha_i^2(\xi_o)}{\sqrt{\sum_{i=1}^{n_f} \alpha_i^4(\xi_o)}} = \frac{\sum_{i=1}^{n_f} \omega_i(\xi_o)}{\sqrt{\sum_{i=1}^{n_f} \omega_i^2(\xi_o)}} \tag{32}$$

where $\alpha_i^2(\xi_o)$ represents the i -th frequency parameter when the mass is located at ξ_o , while $\omega_i(\xi_o)$ is the corresponding cyclic frequency and n_f is the number of measured frequencies included in the summation.

In Fig. 9 the cumulative frequency parameters vs the mass position is reported when five frequencies are accounted for. It can be seen clearly that the cumulative parameter also shows a frequency shift for the body possessing rotary inertia (continuous line) whose intensity is expected to be variable as the number of frequencies included in Eq. (32) changes, as analyzed later in this paper.

In order to assess the influence of the location of the roving body with respect to the crack position on the dynamics of a single cracked beam, in Fig. 10 the variations of the first five frequencies against the locations of the mass, ξ_o , and the crack, ξ_1 , for $m_o = 0.05, \varepsilon = 0.1$ and $\lambda_1 = 1$, are presented. The surfaces show a jump along the vertical plane $\xi_o = \xi_1$ i.e. when the body and crack are coincident, irrespective of the locations of the body and the crack.

In Fig. 11, in order to account for all the considered frequencies, a surface showing the variation of the cumulative frequency parameter $c(\xi_o, \xi_1)$, computed according to Eq. (32), with the locations of the mass and crack ξ_o, ξ_1 , respectively, is shown. Again, the cumulative frequency parameter (computed on the basis of the first five frequencies) is able to enhance the effect of the crack by showing a frequency shift line.

Thus, Figs. 10 and 11 provide a complete trend of the frequencies' jumps at the crack location if the rotary inertia effect of the roving body is accounted for.

In Fig. 12 the dependency of the frequency jump from various parameters to assess their influence on the dynamic behaviour of a single cracked beam is studied. In particular, by considering the i -th frequency parameter at the left (α_i^-) and right (α_i^+) sides of the crack (located at ξ_1), and the corresponding frequency parameter (α_i^o)² in absence of any additional mass, the following normalized frequency jump parameter $\Delta\alpha_i^2$ is plotted in Fig. 12:

$$\Delta\alpha_i^2 = \frac{(\alpha_i^+)^2 - (\alpha_i^-)^2}{(\alpha_i^o)^2} \tag{33}$$

The parametric study reported in Fig. 12 is concerning with the clamped-clamped case reported in Fig. 5 (i.e. $\xi_1 = 0.7, \lambda_1 = 1, m_o = 0.05, \varepsilon = 0.1$).

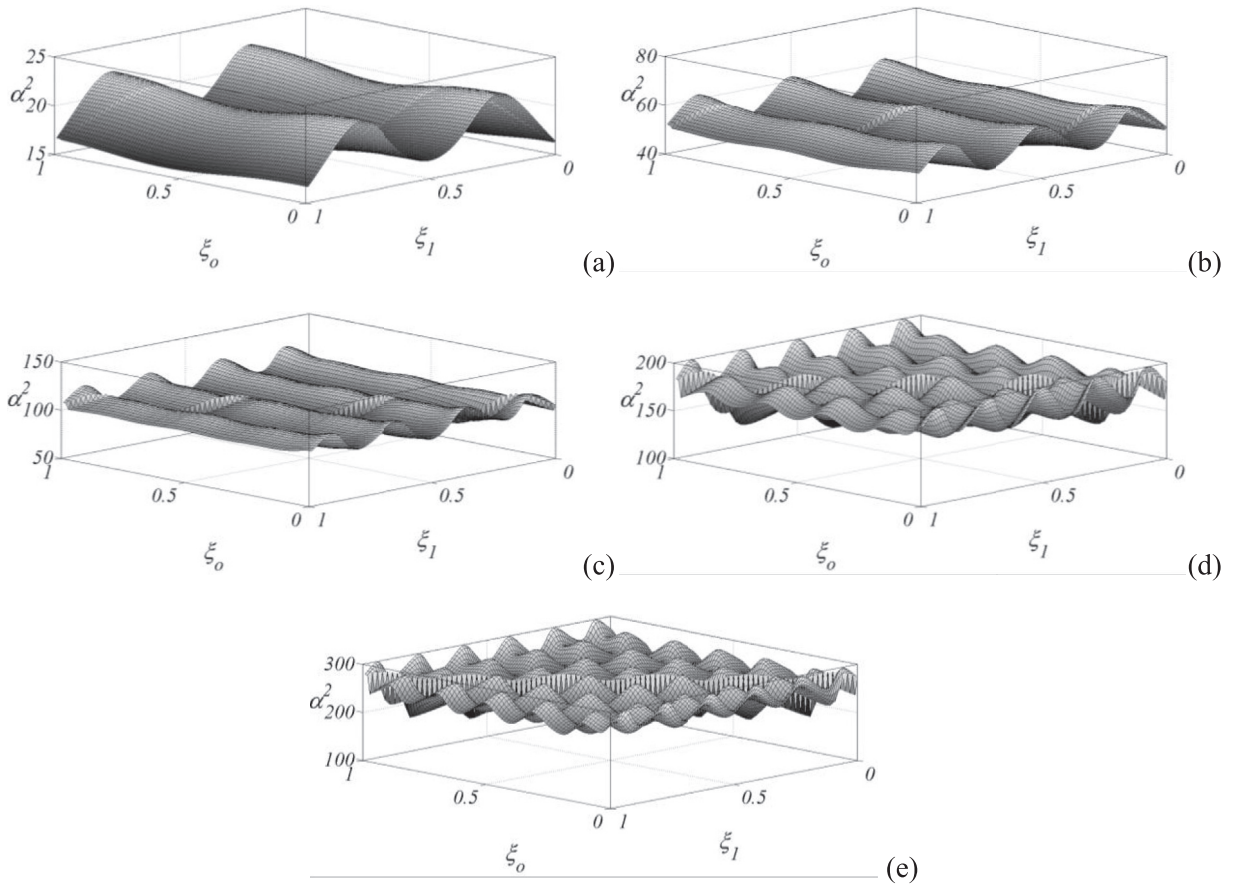


Fig. 10. Single cracked clamped-clamped beam, variable positions of the roving body ($m_0 = 0.05$ $\epsilon = 0.1$) and crack ($\lambda_1 = 1$): first five frequencies.

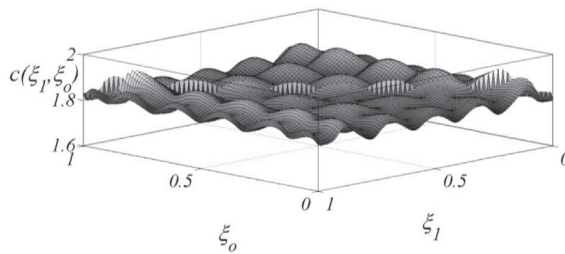


Fig. 11. Single cracked clamped-clamped beam, variable positions of the roving body ($m_0 = 0.05$ $\epsilon = 0.1$) and crack ($\lambda_1 = 1$): cumulative frequency parameter.

In Fig. 12a the normalized frequency jump is shown as a function of the crack location ξ_1 . Generally speaking the maximum value of the frequency shift increases as higher frequencies are considered. Furthermore, the normalized frequency jump crosses the zero axis for all the frequencies, for reasons of symmetry, when the crack is located at $\xi_1 = 0.5$. Thus, in a symmetrical beam, there will be no frequency shift at a crack if it is located at the centre. This is because, irrespective of the location of the body possessing inertia (whether it is immediately to one side of the crack or the other), the combination of the resulting structures will be physically identical and therefore have the same frequencies. Thus in practical applications involving a completely symmetrical structure, to eliminate the possibility of missing a crack at the centre, some form of asymmetry could be introduced, such as the placement of a second body at a location other than the centre.

Each curve representing the detected frequency jump for different frequency modes oscillates around the zero axis; however, except for the symmetric position corresponding $\xi_1 = 0.5$, they do not attain the zero value contemporarily. It can hence be stated that the performance of the proposed procedure, relying on detection of the mentioned frequency jump, is low in proximity of the zero of the frequency jump parameter $\Delta\alpha^2$ for a specific frequency only. On the other hand, at the same cross sections the performance of other frequencies is definitely higher and can be successfully exploited for crack detection.

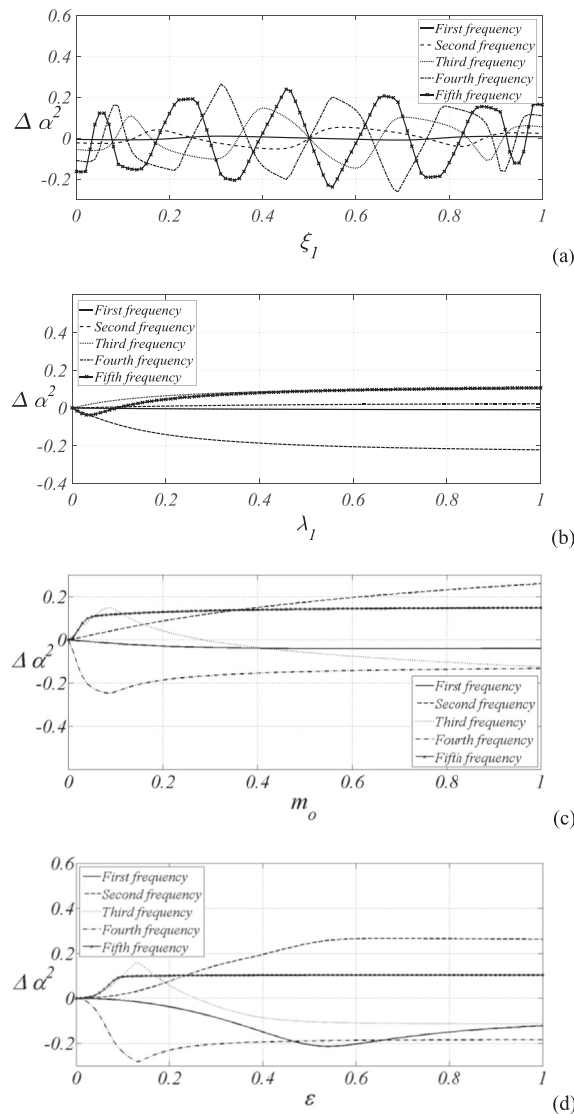


Fig. 12. Single cracked clamped-clamped beam ($\lambda_1 = 1$), relative frequency jumps for the first five frequencies: (a) crack position, (b) crack compliance, (c) mass entity and (d) eccentricity sensitivities.

To this regard it can be concluded that the performance of the procedure does not vary much with the crack position if different frequencies are considered for the jump detection. The trend of the best frequency jump detected for any crack position can hence be provided by the envelope of the $\Delta\alpha^2$ curves plotted in Fig. 12a. Observing Fig. 12a it can hence be stated that for any crack position there will always be a frequency jump parameter reaching the performance ranging roughly between $\pm 15\%$ and $\pm 20\%$ except in the vicinity the symmetric position corresponding to $\xi_1 = 0.5$.

Table 3
Maximum normalized frequency jump at the cracked section for different crack positions over five frequencies ($\lambda_1 = 0.2$, $m_o = 0.05$, $\varepsilon = 0.1$).

ξ_1	Max $\Delta\alpha^2$
0.1	0.1260
0.2	-0.1407
0.3	0.1409
0.4	-0.0871
0.5	0.0000

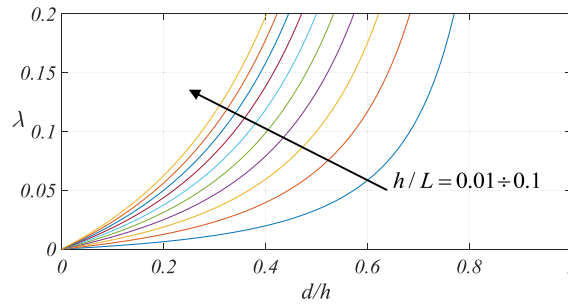


Fig. 13. Crack severity parameter versus normalized crack depth for several values of the beam height to length ratio.

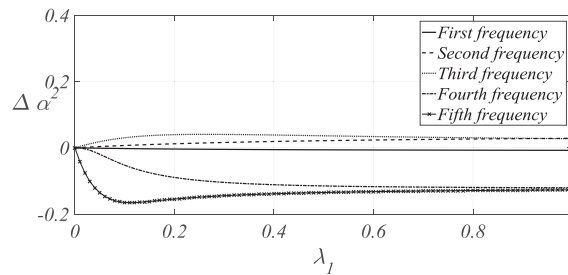


Fig. 14. Single cracked clamped-clamped beam ($\xi_1 = 0.15$, $m_o = 0.05$, $\varepsilon = 0.1$), relative frequency jumps for the first five frequencies vs crack compliance.

In addition, just as a further example, the envelope frequency jump associated to a single cracked beam with $\lambda = 0.2$ are reported for various significant crack locations in Table 3. In this case (once again except for the symmetric position corresponding $\xi_1 = 0.5$ which is associated to no frequency jump) all the considered crack locations are associated to sudden frequency jumps which range from around 9%–14%.

In Fig. 12b the crack compliance has been considered variable in the range $0 \leq \lambda_1 \leq 1$. From a theoretical point of view the procedure is able to detect even small cracks, however, if one were to postulate that a crack can be reasonably detected when the measured frequency jump is equal or higher than a specific limit, say for example, 10% of the corresponding frequency parameter in the absence of any additional mass (i.e. $\Delta\alpha^2 \geq 0.1$), then it is possible to determine the minimum crack depth which would render the crack identifiable using this method. Fig. 12b shows that for the fourth mode, the crack intensity parameter λ must be greater than or equal to 0.1 to ensure that $\Delta\alpha^2 \geq 0.1$. Fig. 12b shows also that the performance of the procedure increases in the range $0.1 \leq \lambda \leq 0.4$ and remains stable for $\lambda > 0.4$.

To give a first rough estimation of the minimum crack depth to be recognized, it is useful to bear in mind that the correspondence between the crack intensity parameter λ and the normalized crack depth d/h can be inferred by choosing a suitable model $K(d/h)$ available in the literature (see for example reference [13]) and depends on the cross section height to the beam length ratio h/L . The dependency between the crack severity λ and the normalized crack depth d/h is reported in Fig. 13 for different values of the cross section height to the beam length ratio h/L , considering the model proposed in Ref. [27]. In view of the above statements the values of the crack depth to height ratio for the curves which correspond to a crack intensity value $\lambda = 0.1$ (corresponding, at least for the case at hand, to 10% frequency jump) can be interpreted as the minimum crack depth for each of the curve giving a range ($[d/h]_{min} \approx 0.25 - 0.65$) dependent on the beam ratio h/L .

Moreover, it is also expected that the range of minimum crack depth for a detectable crack is also dependent on the crack position. In fact, a further example is considered in case a crack is placed at $\xi_1 = 0.15$ and the relevant $\Delta\alpha^2$, λ_1 curves are reported in Fig. 14 for the first five frequencies. The value of λ_1 corresponding to a 10% frequency jump in this case is about $\lambda_1 = 0.05$. The minimum crack depth range dependent on the beam ratio h/L , inferred from Fig. 13, is $[d/h]_{min} \approx 0.18 - 0.58$.

In Fig. 12c the dependence of the normalized frequency jump with respect to the mass ($0 \leq m_o \leq 1$) is considered. Even in this case the trend in the frequency jumps as the mass increases is not always regular, as the third and fourth frequencies demonstrate.

Finally, in Fig. 12d the effect of the eccentricity ($0 \leq \varepsilon \leq 1$) is assessed. Again, the trend of the frequency jump is not always monotonic.

However, it may be seen that irrespective of the values of the mass, crack compliance and effective eccentricity, the frequency parameter shows a noticeable jump at the crack location as long as these values are non-zero, for a beam with a single crack located at $\xi_1 = 0.7$. Repeating this exercise for other crack locations consistently led to the same observations.

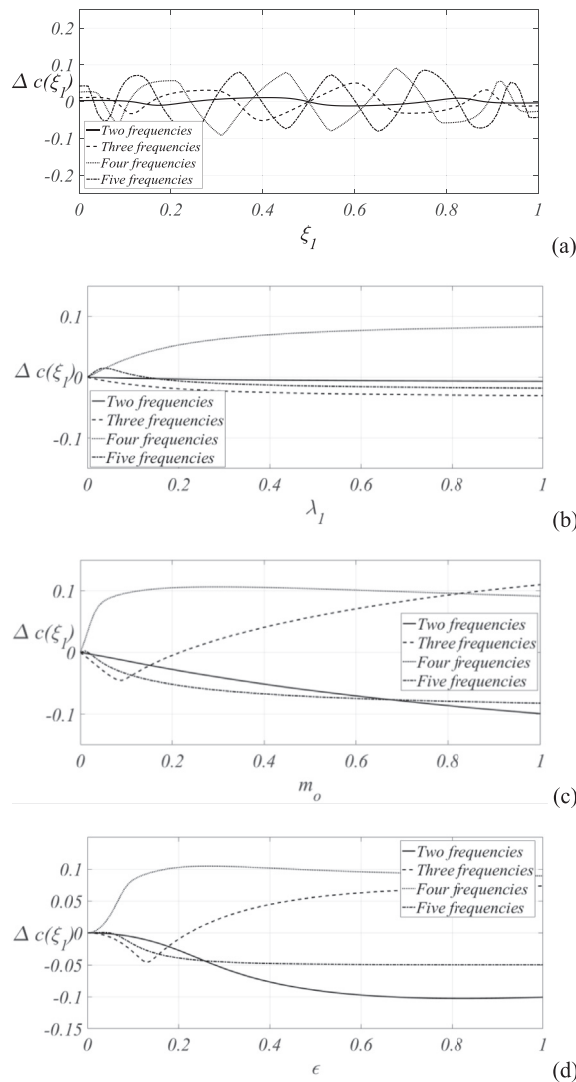


Fig. 15. Single cracked clamped-clamped beam ($\lambda_1 = 1$), cumulative frequency parameter jump vs: (a) crack position, (b) crack compliance, (c) mass entity and (d) eccentricity sensitivities.

Finally, in Fig. 15, the jump of the cumulative frequency parameter (i.e. $\Delta c(\xi_1) = c(\xi_0^+) - c(\xi_0^-)$, when the roving body is located at the right and left sides of the crack) is reported considering the same sensitivity analysis with respect to the parameters investigated in Fig. 12.

In particular, in Fig. 15a, the jump of the cumulative frequency parameter is reported as a function of the crack position for different numbers of frequencies n_f included in the summation in Eq. (32). It is worth noting that each curve has some zero crossing points, which means there are several crack locations which may not lead to any cumulative frequency parameter jump as the mass crosses the crack. These are the points where the slope of the beam in that particular mode is zero and therefore unaffected by the rotary inertia, or in the case that the jumps relative to several frequencies compensate for. However, except when the crack is located at the mid span of the beam, since the zero crossing points for the various modes do not coincide, the proposed detection procedure does not fail. The observation of the desired jump is hence guaranteed. The results reported in Fig. 15a for different crack positions show that the performance of the cumulative frequency parameter in detecting the presence of the crack can be increased by simply accounting for different number of frequencies.

In Fig. 15b, the influence of the crack compliance on the jump of the cumulative frequency parameter is investigated. Analogous considerations to those made for the frequency jump can be made. Of course the performance of the procedure can be improved (as well as the minimum depth of a detectable crack) by taking into account additional numbers of frequencies as can be seen from Figs. 12b and 15b. Generally speaking the detected frequency jump attains values smaller than 10% as the crack intensity parameter λ diminishes.

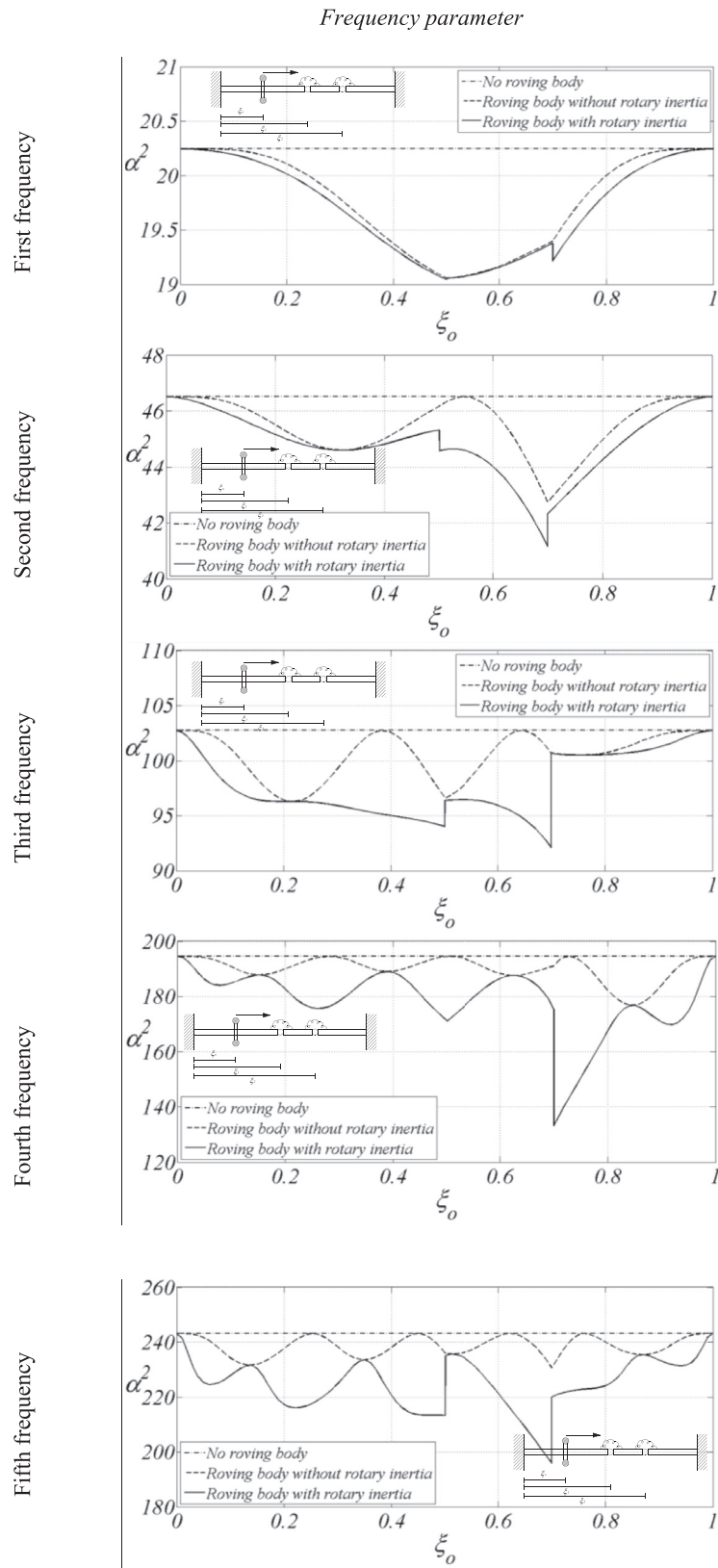


Fig. 16. Frequency parameter α^2 vs position of the roving body for the first five frequencies.

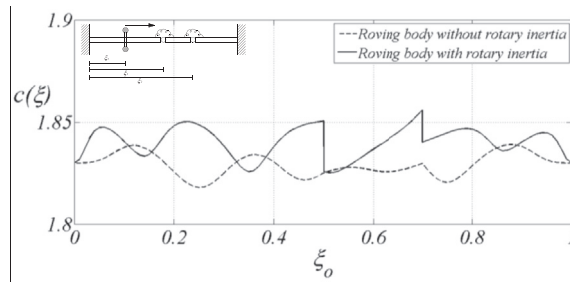


Fig. 17. Double cracked clamped-clamped beam ($\xi_1 = 0.5$ $\xi_2 = 0.7$ $\lambda_1 = 0.1$ $\lambda_2 = 1$), variable position of the mass ($m_o = 0.05$ $\varepsilon = 0.1$): cumulative frequency parameter for the first five frequencies.

An analysis of the effect of the mass is reported in Fig. 15c for values of the normalized mass $0 \leq m_o \leq 1$ for a fixed normalized eccentricity $\varepsilon = 0.1$. Analysis of both Figs. 12c and 15c reveals that for normalized mass of around $m_o = 0.05$, i.e. 5% of the self mass of the beam, and considering an eccentricity equal to $\varepsilon = 0.1$, i.e. 10% of the height of the beam, the performance is already good if four frequencies are considered in the cumulative frequency parameter.

A further evidence of the effect of the normalized mass eccentricity ε is reported in Fig. 15d. Analysis of both Figs. 12d and 15d reveals that for the normalized mass $m_o = 0.05$, i.e. 5% of the self mass of the beam, for an eccentricity of the roving body $\varepsilon \geq 0.1$ (i.e. 10% of the beam length), when four frequencies are considered in the cumulative frequency parameter, the performance of the procedure is satisfactory for the crack detection.

5.4. Double cracked beam

In this sub-section the case of a double cracked beam is considered. The considered application aims to show how the proposed procedure requires the same number of experimental measurements irrespectively of the number of cracks present in the beam. The case of a clamped-clamped beam with two cracks located at $\xi_1 = 0.5$ and $\xi_2 = 0.7$ is presented here as an illustrative example. The crack severities are $\lambda_1 = 0.1$ and $\lambda_2 = 1$, while the characteristics of the roving body are $m_o = 0.05$ and $\varepsilon = 0.1$. In Fig. 14 the first five fundamental frequencies (in terms of the frequency parameter α^2) are plotted against the body position ξ_o . The results are presented for the same three cases and using the same format as in Section 5.1 (i.e. beam without roving body with the dash dot line, beam with a roving body without the rotary inertia effect with the dashed line and beam with a body possessing mass and rotary inertia with the continuous line). Since the healthy beam case has already been presented in Section 5.1, it is not reproduced here.

From the results in Fig. 16 it may be seen that the rotary inertia causes a sudden jump in the frequency – roving body location plots as the body crosses each crack, for each considered frequency, irrespectively of the number and severity of the cracks.

Once again, the frequency jump may or may not be sufficiently high to be observed clearly for some of the modes. Therefore, the cumulative frequency parameter introduced in Eq. (32) is computed again and plotted in Fig. 17 (accounting for the first five frequencies), as a function of the position of the roving body. When the rotary inertia effect of the roving body is neglected (dashed line) only kinks (sharp points) are encountered at the crack locations, while abrupt jumps of the measured frequency can be recognized when the rotary inertia of the roving body is considered (continuous line).

5.5. Multi-cracked beam

Finally, in order to show how the proposed procedure is effective even in the presence of a large number of cracks, a clamped-clamped beam with $n = 10$ equally spaced cracks is investigated. All the cracks have the same severity ($\lambda_i = 0.1$), while the mass and eccentricity are $m_o = 0.05$ and $\varepsilon = 0.1$, respectively.

In Fig. 16 the first five fundamental frequencies (in terms of the frequency parameter α^2) are shown as a function of the body position ξ_o for the cracked beam. The same three different cases as in the previous applications are considered.

The results in Fig. 18 show how, even in the presence of a considerable number of cracks, the abrupt jump due to the rotary inertia effect can be easily noticed at each passage of the roving body over each crack. The variation of the cumulative frequency parameter on the roving body position (accounting for the first five frequencies), when the rotary inertia effect is included, is plotted in Fig. 19 showing that discontinuities are triggered at the crack locations.

6. Conclusions

A novel procedure for identifying the crack locations in beams, that makes use of the effect of the rotary inertia of a roving body on the natural frequencies of a beam as it passes a crack, has been presented. A proof based on the Dynamic Stiffness Matrix and numerical results for specific beams showed that: a roving body possessing rotary inertia introduces a discontinuity in the frequency vs roving body location relationship at crack locations if the crack allows a relative rotation between

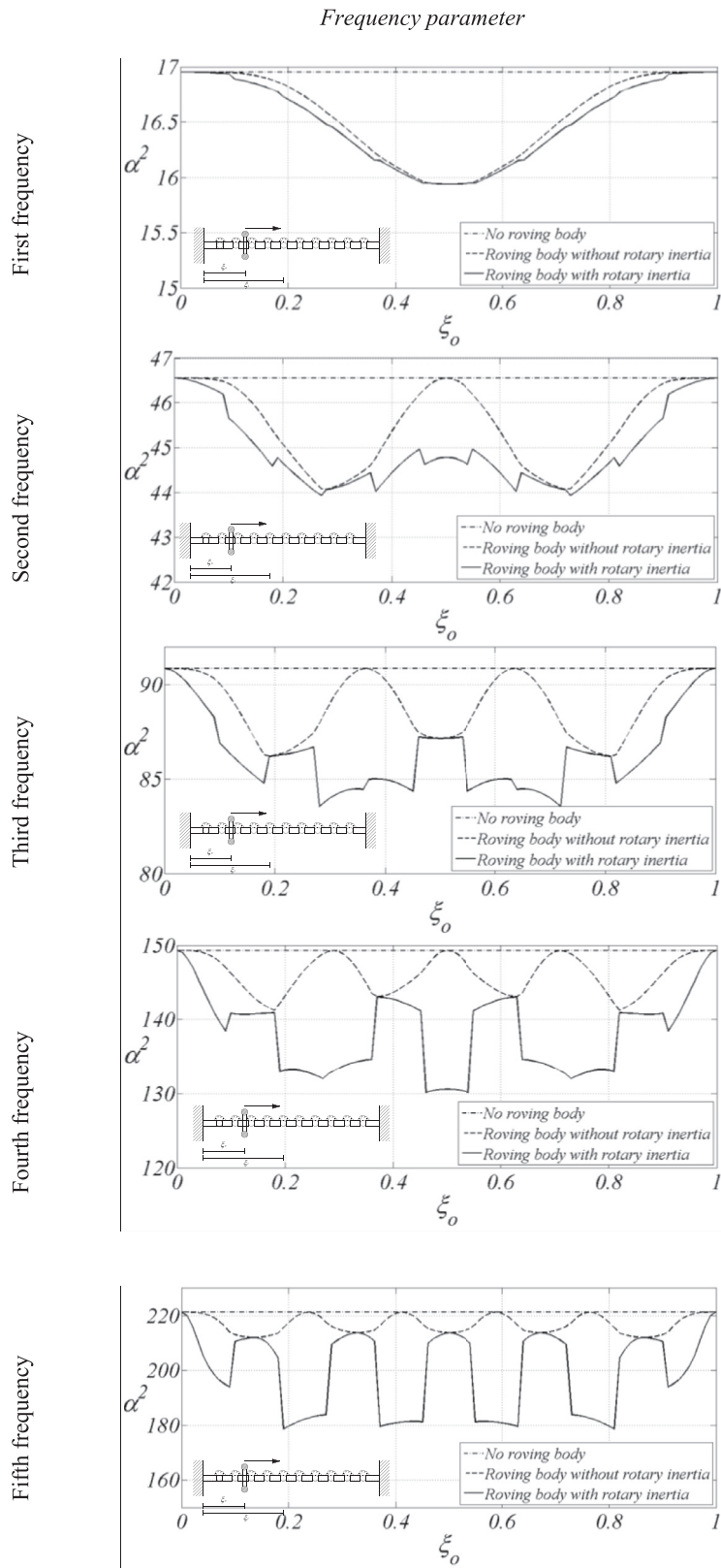


Fig. 18. Frequency parameter α^2 vs roving body position for the first five frequencies.

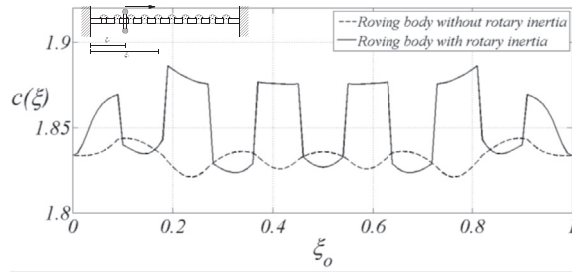


Fig. 19. Clamped-clamped beam with 10 equally spaced cracks ($\lambda_i = 0.1$), variable position of the roving body ($m_o = 0.05$ $e = 0.1$): cumulative frequency parameter for the first five frequencies.

adjacent sections, except at positions that lie on a line of structural symmetry. Furthermore, due to the inertial resistance moment arising from the product of the inertia and the square of the frequency, the magnitude of discontinuity in the frequency vs roving body location plots increases with mode number.

Numerical evidence of the above proof have been provided for beams with single and multiple cracks by presenting a novel closed form solution for multiple cracked beams with an additional body possessing mass and rotary inertia that allows a straightforward parametric analysis requiring the evaluation of the boundary conditions only.

Several procedures aiming at the damage identification in beam-like structures (e.g. bridges, pipeline systems) are based on the use of an additional mass to magnify the variations of the dynamic properties of the structures due to the presence of damage. Such theories are based on the additional translational inertia provided by the roving body. The exploitation of the frequency jump introduced by a roving body endowed with a significant rotary inertia, brought to light in this work, opens new perspectives on the dynamic damage identification. In fact, the proposed methodology is based on a clear and straightforward property directly based on frequency measurements and offers identification of the location using a procedure that is independent of severity and experimental uncertainties.

Acknowledgements

This work is part of the National Research Project "Advanced mechanical modelling of new materials and structures for the solution of 2020 Horizon challenges" (2017–2020), supported by MIUR, Grant No. 2015JW9NJT, Scientific coordinator, prof. M. Di Paola, prot. n. 2015JW9NJT_017.

APPENDIX. Exact integration procedure of Eq. (23)

Laplace transform $L\{\bullet\}$ of the governing equation of the multi-cracked beam in presence of a concentrated mass with rotary inertia given by Eq. (23) is as follows:

$$s^4 \phi(s) - s^3 \phi(0) - s^2 \phi^I(0) - s \phi^{II}(0) - \phi^{III}(0) - \alpha^4 \phi(s) = \alpha^4 m_o \phi(\xi_o) e^{-s\xi_o} - \alpha^4 m_o \epsilon^2 \phi^I(\xi_o) s e^{-s\xi_o} + \sum_{i=1}^n \lambda_i \phi^{II}(\xi_i) s^2 e^{-s\xi_i} \tag{A1}$$

where $\phi(s) = L\{\phi(\xi)\}$, and the variable s represents the complex frequency variable introduced to perform the Laplace transform.

After simple algebra, Eq. (A1) can be given the following form:

$$\phi(s) = \frac{1}{s^4 - \alpha^4} \left[s^3 \phi(0) + s^2 \phi^I(0) + s \phi^{II}(0) + \phi^{III}(0) + \alpha^4 m_o \phi(\xi_o) e^{-s\xi_o} - \alpha^4 m_o \epsilon^2 \phi^I(\xi_o) s e^{-s\xi_o} + \sum_{i=1}^n \lambda_i \phi^{II}(\xi_i) s^2 e^{-s\xi_i} \right] \tag{A2}$$

And, conveniently collecting common terms, Eq. (A2) becomes:

$$\phi(s) = \frac{s^3}{s^4 - \alpha^4} \phi(0) + \frac{s^2}{s^4 - \alpha^4} \phi^I(0) + \frac{s}{s^4 - \alpha^4} \phi^{II}(0) + \frac{1}{s^4 - \alpha^4} \phi^{III}(0) + \alpha^4 m_o \phi(\xi_o) \frac{1}{s^4 - \alpha^4} e^{-s\xi_o} - \alpha^4 m_o \epsilon^2 \phi^I(\xi_o) \frac{s}{s^4 - \alpha^4} e^{-s\xi_o} + \sum_{i=1}^n \lambda_i \phi^{II}(\xi_i) \frac{s^2}{s^4 - \alpha^4} e^{-s\xi_i} \tag{A3}$$

The inverse Laplace transform $L^{-1}\{\bullet\}$ of Eq. (A3) provides the following expression for the displacement function $\phi(\xi)$:

$$\begin{aligned} \phi(\xi, \alpha) = & \widehat{h}_1(\xi, \alpha)\phi(0) + \widehat{h}_2(\xi, \alpha)\phi'(0) + \widehat{h}_3(\xi, \alpha)\phi''(0) + \widehat{h}_4(\xi, \alpha)\phi'''(0) + \\ & + \overline{h}_0(\xi, \alpha)\alpha^4 m_0 \phi(\xi_0, \alpha) + \overline{h}_R(\xi, \alpha)\alpha^4 m_0 e^2 \phi^I(\xi_0, \alpha) + \sum_{i=1}^n \overline{h}_i(\xi, \alpha)\lambda_i \phi^{II}(\xi_i, \alpha) \end{aligned} \tag{A4}$$

where

$$\begin{aligned} \widehat{h}_1(\xi, \alpha) &= \frac{1}{2}(\cos \alpha\xi + \cosh \alpha\xi) \\ \widehat{h}_2(\xi, \alpha) &= \frac{1}{2\alpha}(\sin \alpha\xi + \sinh \alpha\xi) \\ \widehat{h}_3(\xi, \alpha) &= \frac{1}{2\alpha^2}(-\cos \alpha\xi + \cosh \alpha\xi) \\ \widehat{h}_4(\xi, \alpha) &= \frac{1}{2\alpha^3}(-\sin \alpha\xi + \sinh \alpha\xi) \end{aligned} \tag{A5}$$

while $\overline{h}_0(\xi, \alpha)$, $\overline{h}_R(\xi, \alpha)$, $\overline{h}_i(\xi, \alpha)$ are those provided in Eq. (26).

Eq. (A4) can also be written in a more compact implicit form as follows:

$$\begin{aligned} \phi(\xi, \alpha) = & C_1 h_1(\xi, \alpha) + C_2 h_2(\xi, \alpha) + C_3 h_3(\xi, \alpha) + C_4 h_4(\xi, \alpha) + \\ & + \overline{h}_0(\xi, \alpha)\alpha^4 m_0 \phi(\xi_0, \alpha) + \overline{h}_R(\xi, \alpha)\alpha^4 m_0 e^2 \phi^I(\xi_0, \alpha) + \sum_{i=1}^n \overline{h}_i(\xi, \alpha)\lambda_i \phi^{II}(\xi_i, \alpha) \end{aligned} \tag{A6}$$

where $h_1(\xi, \alpha)$, $h_2(\xi, \alpha)$, $h_3(\xi, \alpha)$, $h_4(\xi, \alpha)$ are given in Eq. (26) and the integration constants C_1, C_2, C_3, C_4 , related to the values $\phi(0), \phi'(0), \phi''(0), \phi'''(0)$, have been defined as follows:

$$\begin{aligned} C_1 &= \frac{1}{2\alpha} \left[\phi'(0) - \frac{1}{\alpha^2} \phi'''(0) \right] \\ C_2 &= \frac{1}{2} \left[\phi(0) - \frac{1}{\alpha^2} \phi''(0) \right] \\ C_3 &= \frac{1}{2\alpha} \left[\phi'(0) + \frac{1}{\alpha^2} \phi'''(0) \right] \\ C_4 &= \frac{1}{2} \left[\phi(0) + \frac{1}{\alpha^2} \phi''(0) \right] \end{aligned} \tag{A7}$$

The recursive implicit expression reported in Eq. (A6) needs the evaluation of $\phi(\xi_0, \alpha)$, $\phi^I(\xi_0, \alpha)$ and $\phi^{II}(\xi_i, \alpha)$, which can be calculated, in view of Eq. (26), as follows:

$$\begin{aligned} \phi(\xi_0, \alpha) &= C_1 h_1(\xi_0, \alpha) + C_2 h_2(\xi_0, \alpha) + C_3 h_3(\xi_0, \alpha) + C_4 h_4(\xi_0, \alpha) + \sum_{i=1}^{i_0} \overline{h}_i(\xi_0, \alpha)\lambda_i \phi^{II}(\xi_0, \alpha) \\ \phi^I(\xi_0, \alpha) &= C_1 h_1^I(\xi_0, \alpha) + C_2 h_2^I(\xi_0, \alpha) + C_3 h_3^I(\xi_0, \alpha) + C_4 h_4^I(\xi_0, \alpha) + \sum_{i=1}^{i_0} \overline{h}_i^I(\xi_0, \alpha)\lambda_i \phi^{II}(\xi_i, \alpha) \\ \phi^{II}(\xi_i, \alpha) &= C_1 h_1^{II}(\xi_i, \alpha) + C_2 h_2^{II}(\xi_i, \alpha) + C_3 h_3^{II}(\xi_i, \alpha) + C_4 h_4^{II}(\xi_i, \alpha) + \\ & + \overline{h}_0^{II}(\xi_i, \alpha)\alpha^4 m_0 \phi(\xi_i, \alpha) + \overline{h}_R^{II}(\xi_i, \alpha)\alpha^4 m_0 e^2 \phi^I(\xi_0, \alpha) + \sum_{k=1}^{i-1} \overline{h}_k^{II}(\xi_i, \alpha)\lambda_k \phi^{II}(\xi_k, \alpha) \end{aligned} \tag{A8}$$

where i_0 is associated to the last crack positioned on the left of the mass (i.e. for $i < i_0 \rightarrow \xi_i < \xi_0$). By replacing $\phi_j(\xi_0, \alpha)$, $\phi_j^I(\xi_0, \alpha)$, $\phi_j^{II}(\xi_i, \alpha)$ in Eq. (A6) the following closed form of the solution (reported in the main body of this paper as Eq. (24)) can be provided:

$$\phi(\xi, \alpha) = C_1 f_1(\xi, \alpha) + C_2 f_2(\xi, \alpha) + C_3 f_3(\xi, \alpha) + C_4 f_4(\xi, \alpha) \tag{A9}$$

where

$$f_j(\xi, \alpha) = h_j(\xi, \alpha) + \bar{h}_o(\xi, \alpha)\alpha^4 m_o f_j(\xi_o, \alpha) + \bar{h}_R(\xi, \alpha)\alpha^4 m_o e^2 f_j^I(\xi_o, \alpha) + \sum_{k=1}^n \bar{h}_k(\xi, \alpha)\lambda_k f_j^{II}(\xi_k, \alpha), \quad j = 1, \dots, 4 \quad (\text{A10})$$

It is worth to notice that, although the functions $f_j(\xi, \alpha)$, given by Eq. (A10), depends formally on the unknown terms $f_j(\xi_o, \alpha)$, $f_j^I(\xi_o, \alpha)$, $f_j^{II}(\xi_k, \alpha)$, it has to be clarified that the latter terms can be straightforwardly evaluated by the same Eq. (A10) and accounting for Eq. (26).

In fact, for $\xi = \xi_o \rightarrow \bar{h}_o(\xi_o, \alpha) = \bar{h}_R(\xi_o, \alpha) = 0$, hence:

$$f_j(\xi_o, \alpha) = h_j(\xi_o, \alpha) + \sum_{k=1}^{i_o} \bar{h}_k(\xi_o, \alpha)\lambda_k f_j^{II}(\xi_k, \alpha), \quad j = 1, \dots, 4 \quad (\text{A11})$$

then, for $\xi = \xi_o \rightarrow \bar{h}_o^I(\xi_o, \alpha) = \bar{h}_R^I(\xi_o, \alpha) = 0$, hence:

$$f_j^I(\xi_o, \alpha) = h_j^I(\xi_o, \alpha) + \sum_{k=1}^{i_o} \bar{h}_k^I(\xi_o, \alpha)\lambda_k f_j^{II}(\xi_k, \alpha), \quad j = 1, \dots, 4 \quad (\text{A12})$$

while for $\xi = \xi_k$:

$$f_j^{II}(\xi_k, \alpha) = h_j^{II}(\xi, \alpha) + \bar{h}_o^{II}(\xi, \alpha)\alpha^4 m_o f_j(\xi_o, \alpha) + \bar{h}_R^{II}(\xi, \alpha)\alpha^4 m_o e^2 f_j^I(\xi_o, \alpha) + \sum_{i=1}^{k-1} \bar{h}_i^{II}(\xi, \alpha)\lambda_i f_j^{II}(\xi_i, \alpha), \quad j = 1, \dots, 4 \quad (\text{A13})$$

Eqs. (A11)–(A13) show that each of the terms $f_j(\xi_o, \alpha)$, $f_j^I(\xi_o, \alpha)$, $f_j^{II}(\xi_k, \alpha)$ depend on the values of the same quantity evaluated at the previous discontinuity cross sections.

References

- [1] S.W. Doebling, C.R. Farrar, M.B. Prime, D.W. Shevitz, Damage Identification and Health Monitoring of Structural and Mechanical Systems from Changes in Their Vibration Characteristics: a Literature Review (LA-13070-MS), Los Alamos National Laboratory, Los Alamos, NM, 1996.
- [2] S.W. Doebling, C.R. Farrar, M.B. Prime, A summary review of vibration-based damage identification methods, Shock Vib. Digest 30 (2) (1998) 91–105.
- [3] M. Solís, A.J. Benjumea, M. Algaba, P. Galvín, Analysis of stationary roving mass effect for damage detection in beams using wavelet analysis of mode shapes, in: Journal of Physics: Conference Series, 628(1), IOP Publishing, 2015, p. 012014.
- [4] A. Pandey, M. Biswas, M. Samman, Damage detection from changes in curvature mode shapes, J. Sound Vib. 145 (2) (1991) 321–332.
- [5] S. Caddemi, I. Calió, Exact reconstruction of multile concentrated damages on beams, Acta Mech. 225 (11) (2014) 3137–3156.
- [6] S. Zhong, S.O. Oyadiji, Identification of cracks in beams with auxiliary mass spatial probing by stationary wavelet transform, J. Vib. Acoust. 130 (4) (2008) 1–14.
- [7] A. Bahador, S.O. Oyadiji, Use of the roving mass technique and SWT to identify and locate multiple cracks in simply-supported beams, vibration engineering and technology of machinery, Mech. Mach. Sci. 23 (2015) 253–263.
- [8] S. Zhong, S.O. Oyadiji, Analytical predictions of natural frequencies of cracked simply supported beams with a stationary roving mass, J. Sound Vib. 311 (1) (2008) 328–352.
- [9] J. De Los Rios, S. Ilanko, D. Kennedy, Decoupling severity and location from cracked beams, in: The 23rd International Congress on Sound and Vibration, Athens, Greece, 2016.
- [10] T. Chondros, A. Dimarogonas, J. Yao, A continuous cracked beam vibration theory, J. Sound Vib. 215 (1) (1998) 17–34.
- [11] A. Labib, D. Kennedy, C. Featherston, Free vibration analysis of beams and frames with multiple cracks for damage detection, J. Sound Vib. 333 (20) (2014) 4991–5003.
- [12] S. Ilanko, Introducing the use of positive and negative inertial functions in asymptotic modelling, Royal Soc. Proc. A 461 (2005) 2545–2562.
- [13] S. Caddemi, I. Calió, F. Cannizzaro, D. Rapicavoli, A novel beam finite element with singularities for the dynamic analysis of discontinuous frames, Arch. Appl. Mech. 83 (10) (2013) 1451–1468.
- [14] S. Caddemi, I. Calió, F. Cannizzaro, Closed-form solutions for stepped Timoshenko beams with internal singularities and along-axis external supports, Arch. Appl. Mech. 83 (2013) 559–577.
- [15] S. Caddemi, I. Calió, F. Cannizzaro, The influence of multiple cracks on tensile and compressive buckling of shear deformable beams, Int. J. Solids Struct. 50 (2013) 3166–3183.
- [16] S. Caddemi, I. Calió, F. Cannizzaro, Flutter and divergence instability of the multi-cracked cantilever beam column, J. Sound Vib. 333 (2014) 1718–1733.
- [17] S. Caddemi, I. Calió, F. Cannizzaro, Influence of an elastic end support on the dynamic stability of Beck's column with multiple weak sections, Int. J. Non Lin. Mech. 69 (2015) 14–28.
- [18] F. Cannizzaro, J. De Los Rios, S. Caddemi, I. Calió, S. Ilanko, Crack localization in beams by frequency shifts due to roving mass with rotary inertia, Procedia Eng. 199 (2017) 900–905.
- [19] S. Fekrazadeh, N. Khaji, An analytical method for crack detection of Timoshenko beams with multiple open cracks using a test mass, Eur. J. Environ. Civil Eng. 21 (1) (2017) 24–41.
- [20] Q. Wang, X. Deng, Damage detection with spatial wavelets, Int. J. Solid Struct. 36 (1999) 927–939.
- [21] S. Quek, Q. Wang, L. Zhang, K. Ang, Sensitivity analysis of crack detection in beams by wavelet technique, Int. J. Mech. Sci. 43 (2001) 2899–2910.
- [22] E. Douka, S. Loutridis, A. Trochidis, Crack identification in beams using wavelet analysis, Int. J. Solid Struct. 40 (2003) 3557–3569.
- [23] P.D. Spanos, G. Failla, A. Santini, M. Pappaticò, Damage detection in Euler Bernoulli beams via spatial wavelet analysis, Struct. Contr. Health Monit. 13 (2006) 472–487.

- [24] J. Wang, P. Qiao, On irregularity-based damage detection method for cracked beams, *Int. J. Solid Struct.* 45 (2008) 688–704.
- [25] S. Zhong, J. Zhong, Q. Zhang, N. Maya, Quasi-optical coherence vibration tomography technique for damage detection in beam-like structures based on auxiliary mass induced frequency shift, *Mech. Syst. Signal Process.* 93 (2017) 241–254.
- [26] CSI Analysis Reference Manual for SAP2000, Computers and Structures Inc., 2007.
- [27] C. Bilello, Theoretical and Experimental Investigation on Damaged Beams under Moving Systems, Ph.D. thesis, Università degli Studi di Palermo, Palermo, Italy, 2001.
- [28] J. Fernández-Sáez, A. Morassi, L. Rubio, Crack identification in elastically restrained vibrating rods, *Int. J. Non Lin. Mech.* 94 (2016) 257–267.